

**Gwenael LE GAL**

**Filière Physique - Nanosciences  
2016/2017**

**National Enterprise for nanoScience and nanoTechnology NEST  
Piazza San Silvestro 12, 56127 Pisa, Italy**

# Ohmic contact engineering and low temperature magneto-transport measurements in few-layer Black Phosphorus

du 01/05/17 au 31/07/17

**Sous la supervision de :**

- **Maître de stage : Dr Stefan HEUN, stefan.heun@nano.cnr.it**
- **Dr Francesca TELESIO, francesca.telesio@nano.cnr.it**
- **Tuteur école :**

Confidentialité : non

**Ecole nationale  
supérieure de physique,  
électronique, matériaux**

**Phelma**  
Bât. Grenoble INP - Minatec  
3 Parvis Louis Néel - CS 50257  
F-38016 Grenoble Cedex 01

Tél +33 (0)4 56 52 91 00  
Fax +33 (0)4 56 52 91 03

**<http://phelma.grenoble-inp.fr>**

# Contents

Acknowledgements .....	2
Glossary .....	3
List of Figures.....	4
Introduction .....	5
1 Black Phosphorus presentation and state of the art .....	6
1.1 Semiconducting Black Phosphorus.....	6
1.2 Metal-semiconductor contact and field-effect transistor .....	8
1.3 Black phosphorus field-effect transistor .....	11
2 Sample fabrication process.....	15
2.1 Black Phosphorus' exfoliation.....	15
2.2 Device design.....	16
2.2.1 Electron Beam Lithography.....	17
2.2.2 Thermal evaporation.....	18
3 Measurements and analysis .....	20
3.1 Experimental setup.....	20
3.2 Electrical contact engineering.....	21
3.3 Transport measurements as a function of gate voltage.....	28
4 Summary.....	31
4.1 Conclusion .....	31
References .....	32
4.2 Abstract.....	34
4.3 Résumé.....	34

## Acknowledgements

These three months I spent in Pisa at the National Enterprise for nanoScience and nanotechnology (NEST) laboratory were for me an excellent period of learning. I would like to thank everyone I met during this internship at the laboratory.

I would first like to thank my supervisor, Dr Stefan HEUN for his warm welcome when I arrived and his precious advices and support for the good leading of the project.

I would also like to thank Dr Francesca TELESIO, with whom I worked every day during these months on the project, for everything she taught me, the time she dedicated to me and her wonderful implication in the project that made this work a pleasure.

I am really grateful for having worked with you both on this project.

## Glossary

<b>2D</b> : Two-Dimensional	5, 23, 31
<b>AC</b> : Alternative signal	20
<b>bP</b> : Black Phosphorus	5, 6, 7, 11, 13, 14, 20, 27, 30, 34
<b>CVD</b> : Chemical Vapor Deposition	7
<b>DC</b> : Direct signal	20
<b>EBL</b> : Electron Beam Lithography	15, 17, 19
<b>FET</b> : Field-Effect Transistor	5, 12, 13, 14, 15, 20, 27, 31, 34
<b>I-V</b> : Current versus Voltage characteristic	20, 21, 22
<b>M-SC</b> : Metal-Semiconductor	8, 10, 12, 13
<b>MAA</b> : Methacrylic Acid	16
<b>MMA</b> : Methyl-Methacrylate	16, 17, 18
<b>MOS</b> : Metal Oxide Semiconductor	9, 10
<b>PMMA</b> : Poly(Methyl-Methacrylate)	16, 17, 18
<b>SEM</b> : Scanning Electron Microscope	17
<b>TLM</b> : Transfer Length Method	13, 20, 21, 22, 24, 26
<b>TMD</b> : Transition Metal Dichalcogenide	5, 31

## List of Figures

Figure 1: (a) Side view and (b) top view of black phosphorus crystal structure [4] .....	6
Figure 2: Black-phosphorus band gap versus number of layers, from [5] .....	7
Figure 3: Schematic metal-semiconductor junction's band diagram for a P-type semiconductor with $\Phi_M > \Phi_{SC}$ . .....	8
Figure 4: Schematic metal-semiconductor junction's band diagram for a P-type semiconductor with $\Phi_M < \Phi_{SC}$ . .....	9
Figure 5: Schematic representation of a back-gated field-effect transistor. ....	10
Figure 6 : Band diagram of a field-effect transistor for a p-doped channel with (a) $\Phi_M > \Phi_{SC}$ and (b) $\Phi_M < \Phi_{SC}$ . We consider here a long enough channel so that the band bending at the drain is not affected by the voltage applied on the source.....	10
Figure 7 : $I_{SD}$ vs $V_g$ characteristics of black phosphorus field-effect transistors at room temperature. ....	12
Figure 8: $I_{SD}$ vs $V_g$ characteristics of black phosphorus field-effect transistors at room temperature with Ti contacts. (a) from [14], (b) from [15] and (c) from [16]. In (b) arrows indicates the y-axis to follow.....	13
Figure 9:Glove bag's picture. The bag is filled with nitrogen and we exfoliate black phosphorus inside.....	15
Figure 10: (a) Optical image (5X) of a designed square. Golden pads around are used to build electrical contacts with the flake. ....	16
Figure 11 : EBL mask designed for the square (a) and the flake (b) from Fig 10.....	18
Figure 12 : Optical images of contacted devices. (a) is 20X magnification, the scale bar represents 50 $\mu\text{m}$ . (b) 100X magnification of the top device of (a). ....	19
Figure 13: Picture of the bouncer showing the needle with Au wire .....	19
Figure 14: I-V curves for three different devices with Chromium, Titanium and Nickel contacts. ....	21
Figure 15: (a) TLM graph for the tick and the thin part of the chromium device at room temperature. Dashed lines are a guide to the eye. (b) Optical microscopy image of the black phosphorus flake where we can see the two different thicknesses. ....	23
Figure 16 : Schematic sketch of current crowding. If the transfer length $L_T$ is small, the carriers travel more in the contact than in the semiconductor. ....	24
Figure 17: TLM graphs of the three samples with Chromium, Titanium and Nickel contacts. Dashed lines are used as a guide to the eye. ....	25
Figure 18: Source-drain current characteristics of our three samples at room and low temperature. Arrows give the direction of sweeping and numbers give the order of the sweeps. The coloured lines are a guide to the eye for the fitted linear regions for field-effect mobility evaluation.....	28
Figure 19: $R$ vs $V_g$ (left) and $C$ vs $V_g$ (right) characteristics of the Ti-contacted device from figure 17. Colored lines on $G$ vs $V_g$ graph are a guide to the eye of the fitted linear region for field-effect mobility. ....	29

# Introduction

During the last decades, electronics devices became usual, even essential in our everyday life. The miscellaneous applications are now more and more demanding in term of calculus' power and decreasing size. In the framework of building devices for different applications than the Silicon-based electronic, it became essential to find new materials. The discovery of two-dimensional (2D) materials like graphene opened a new field of investigation in order to have more powerful and low sized devices. Whereas graphene has many impressive electronic properties, its absence of intrinsic bandgap limits its applications in logic electronics. To solve this issue, other 2D semiconducting materials began to be investigated like transition metal dichalcogenides (TMD) and Black Phosphorus (bP). They both present interesting characteristics to build low sized field-effect transistors (FET) thanks to their layered structure, that also allows to tune their band gap depending on the number of layers. They display intrinsic semiconducting behaviour and a direct band gap in their monolayer form [1], [2]. However, Black Phosphorus has an advantage on TMDs. It is, with graphene, actually, the only monoatomic 2D material. Therefore, a higher carrier mobility can be theoretically expected in bP than in TMDs materials. Black phosphorus is then a good candidate for future low-sized electronics devices thanks to these characteristics.

However, to build efficient field-effect transistors with such promising materials, good physical properties are not the only characteristics that have to be taken into account. Technological aspects, like the contact's behaviour at the interface between the contacting metal and the semiconductor is a critical parameter that determines the performances of such devices. Indeed, this parameter is critical because it rules the carrier injection in the transistor's channel and a good ohmic contact is compulsory for the reliability of the device.

During this three months internship at the NEST laboratory in Pisa, the purpose of the subject is to deduce a good contacting metal to black phosphorus, between three different metals : Chromium (Cr), Titanium (Ti) and Nickel (Ni).

A presentation of this material, the theoretical requirements about metal-semiconductor contact and a brief state of the art concerning black phosphorus field-effect transistors will be given in Chapter 1. At the beginning, the interesting transport properties of the material along with reasons that motivate investigation about it will be detailed, ensuing a presentation of the field-effect transistor and especially the metal-semiconductor contact. Finally, the main research results known up to now concerning black phosphorus FETs will be presented.

Chapter 2 will describe the device fabrication. The different steps of the fabrication process will be detailed with a brief presentation of the different methods used for the most important steps.

The experimental setup, specific understandings for the measurements, and methods used to extract the contact resistance, the field-effect mobility along with the analysis of the performed measurements will be described in Chapter 3.

Finally, a summary of the whole work as well as further discussions about the possible outlooks concerning this study will be given.

# 1 Black Phosphorus presentation and state of the art

## 1.1 Semiconducting Black Phosphorus

Black phosphorus is the most stable allotropic form of the phosphorus (P) element. It has several structural phases: a semiconducting orthorhombic phase at atmospheric pressure, a semimetallic rhombohedral phase from 5 GPa to 10 GPa and a metallic simple cubic phase above 10 GPa [3]. The orthorhombic phase, which is of interest for us, presents a layered structure in which layers are held together by van der Waals interactions. Each atom of phosphorus is bonded to three other atoms by covalent bonds. Each bP layer has a graphene-like honeycomb structure, which indeed is puckered in the case of black phosphorus, as can be seen in Fig.1b. Due to this puckered lattice, two kinds of P-P bonds exist, one is in plane with a 2.224 Å length (A-B and C-D in Fig.1a) and the other out of plane with a 2.244 Å length (B-C in Fig 1a) [4]. The inter-layer distance is about 5.3 Å [4]. This leads to an anisotropic crystal lattice with two directions named “Zigzag”, parallel to the ridges, and “Armchair” perpendicular to the ridges.

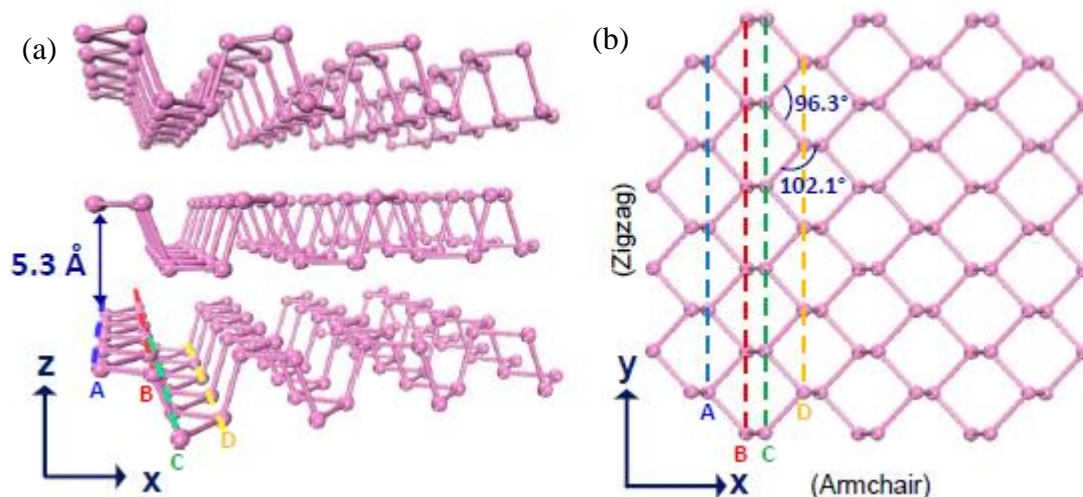


Figure 1: (a) Side view and (b) top view of black phosphorus crystal structure [4]

This phase is semiconducting and it has a direct electronic band gap of 0.3 eV in its bulk form, which can be tuned by the thickness of the bP film until 1-2 eV in the monolayer limit, as shown in Fig. 2, due to a decrease of interlayer interactions [1].

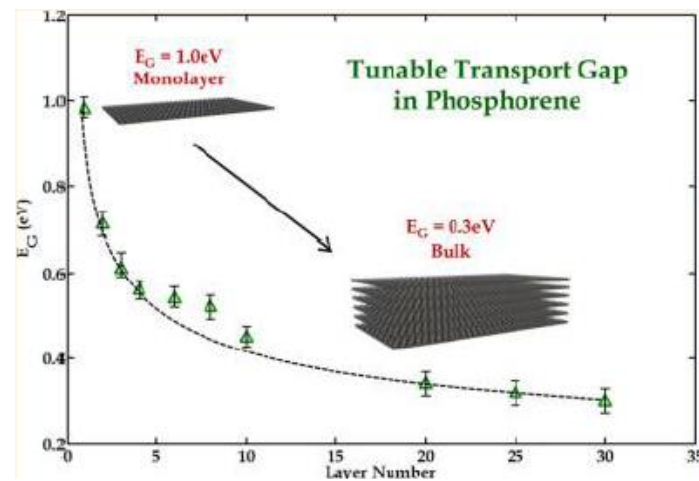


Figure 2: Black-phosphorus band gap versus number of layers, from [5]

This semiconductor is intrinsically p-doped [3] due to the presence of atomic vacancy defects in its structure that create energy levels in the band gap near the valence band top [6]. Moreover, it displays a high hole mobility, up to  $\sim 6000 \text{ cm}^2 \text{ V}^{-1} \text{ s}^{-1}$  [7], also depending on the zigzag or armchair direction [3].

The layered structure allows mechanical exfoliation of few-layers and even single layer, named phosphorene.

Therefore, one can easily understand the interest that arises from this material. On the one hand, the anisotropic lattice induces anisotropy in many properties like Seebeck effect or polarized light depending resonance effects, this makes black phosphorus interesting for thermoelectrical or optical applications. On the other hand, its direct, moderate and tunable band gap combined with its high hole mobility and low size devices' fabrication perspective drive bP a promising material for optoelectronics and micro-electronics.

However, in practice, fabricating devices with black phosphorus encounters some issues. At the beginning of the experiment with bP, during the 1950's, it did not appear to be possible to have single crystals, which was an issue for transport measurement. The first black phosphorus single crystal was obtained in 1981 from the amorphous red phosphorus form under high pressure [3]. Since, researchers have begun to investigate about black phosphorus for its physical and semiconducting properties but was supplanted by other semiconductors for electronics applications. However, since graphene was exfoliated for the first time in the beginning of the twenty-first century [8], black phosphorus had a second birth thanks to its graphite-like layered structure which allows a single-layer exfoliation. Nevertheless, conversely to graphene, phosphorene can only be obtained by exfoliation. No Chemical Vapour Deposition (CVD) or epitaxial growth technics exist yet.

The other main problem concerning black phosphorus is its reactivity with oxygen and water steam, which is significantly increased when exposed to light [9]. Consequently, the device fabrication is difficult and requires a lot of precaution. Nevertheless, with a suitable processing environment, black phosphorus channels based field-effect transistor can be built.



## 1.2 Metal-semiconductor contact and field-effect transistor

In this section, the theoretical requirements about the metal-semiconductor junction (M-SC) will be described, compulsory for the further analysis of the third Chapter. Then, the functioning of a field-effect transistor will be explained, focusing on the important parameters that explain the behaviour of this device.

The metal-semiconductor junction consists in the gathering of a metal and a semiconductor, both characterized by their work function, the difference in energy between the vacuum level and the Fermi level. We will here mainly focus on the case of a p-doped semiconductor, which will be described in both cases when the metal's work function  $\Phi_M$  is higher than the semiconductor's one  $\Phi_{SC}$ , and when  $\Phi_{SC}$  is higher than  $\Phi_M$ . To describe this contact, we will discuss following band diagrams in both situations and with a polarization.

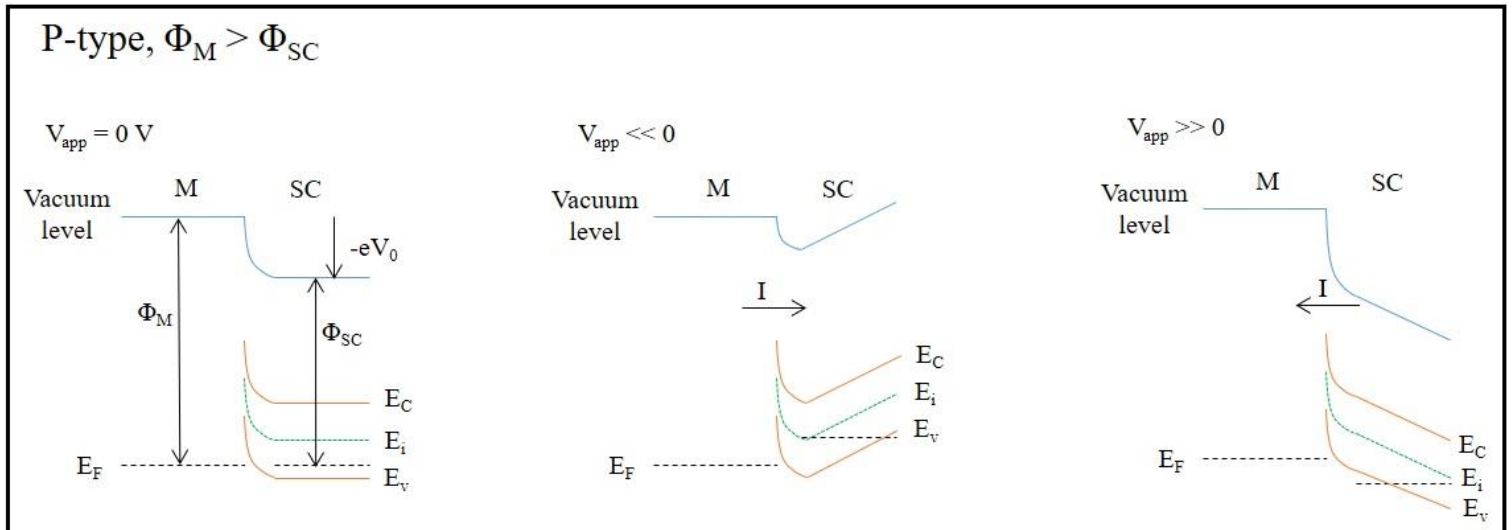


Figure 3: Schematic metal-semiconductor junction's band diagram for a P-type semiconductor with  $\Phi_M > \Phi_{SC}$ . M and SC stand for metal and semiconductor respectively,  $V_{app}$  is the applied voltage on the semiconductor,  $V_0$  the threshold voltage, corresponding to the difference between the two work functions, and  $E_C$ ,  $E_F$ ,  $E_i$  and  $E_v$  are the conduction band bottom energy, the Fermi level energy, the intrinsic Fermi level energy and the valence band top energy respectively.

From this diagram we can deduce that the contact will be ohmic when the metal's work function is larger than the semiconductor's one. At the interface, the top of the valence band comes closer (overcomes here but it is the same) to the Fermi level of the metal. Thus, we are in the accumulation regime for holes, majority carriers in a p-doped semiconductor, there is no Schottky barrier for them. When the applied voltage is positive, the current will be positive, flowing from the semiconductor to the metal. On the other hand, when  $V_{app}$  is negative, the current will be negative as well, flowing from the metal to semiconductor. This current is due to the diffusion and the applied voltage (drift).

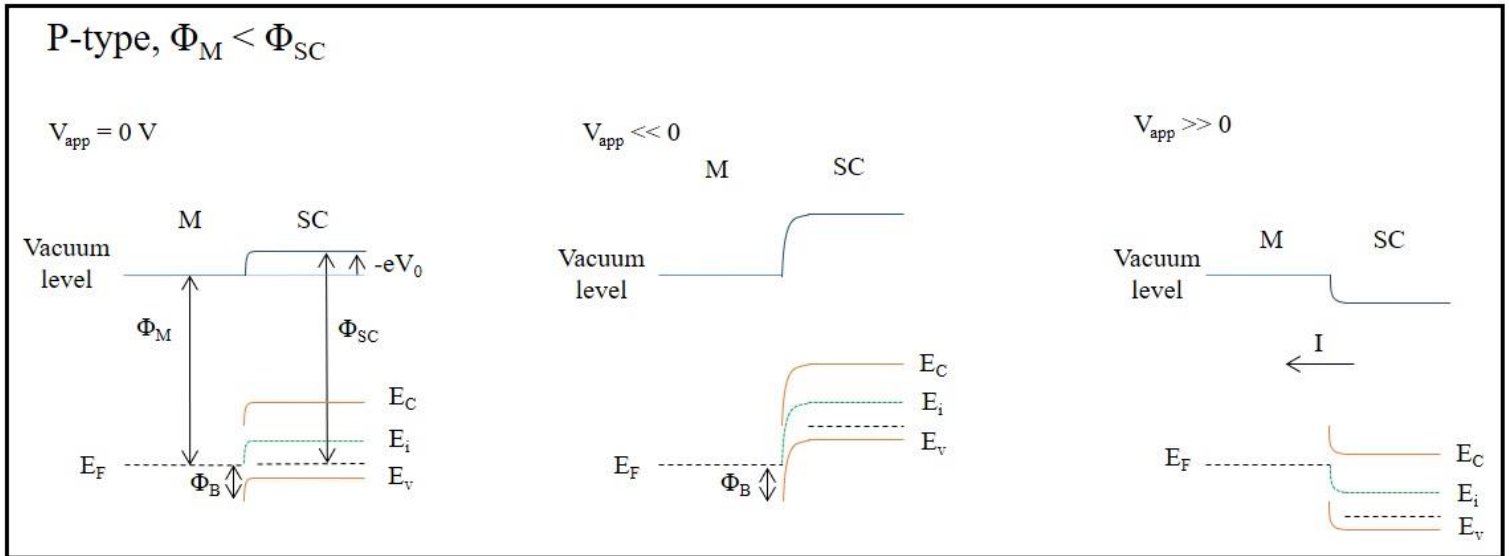


Figure 4: Schematic metal-semiconductor junction's band diagram for a P-type semiconductor with  $\Phi_M < \Phi_{SC}$ .  $\Phi_B$  stands for the Schottky barrier's height in energy. Voltage are applied on the semiconductor.

Here, opposite to the previous case, we can see that the equilibrium state of the junction ( $V_{app} = 0\text{ V}$ ) shows an energetical barrier for holes. Consequently, the band bending at the interface is not favorable for holes and a depletion region appears. This means that, to make holes overcome the barrier and create a current, a minimum voltage is required. This minimum bias is called the flat band voltage and corresponds with the case where bands are not bent ( $V_0$  in Fig. 3 & 4). When there is no band bending, the depletion region disappears, what allows holes to diffuse from the semiconductor to the metal. Moreover, for holes, the drift direction due to the applied voltage is in the same direction as the diffusion flux, so that there is no competition between the diffusion flux and the drift flux. This is the drift-diffusion contribution.

In such junctions, another phenomenon is also creating current : the thermoionic emission. When the temperature is high enough so that the valence band is quite filled with holes, those which have enough energy will be able to overcome the barrier and hence create a current. When the depletion region is thin, for  $V_{app}$  around  $V_0$ , holes can also tunnel through the barrier. Thus between  $-V_0$  and  $V_0$ , there is a small thermoionic emission and tunnel current and a small diffusion flux of electrons, the minority carriers.

From this, we can easily understand that the resistance at the interface of the junction will be affected by the nature of the contact, ohmic or Schottky, but also by the predominant mechanism creating the current. An ohmic contact should provide a better contact resistance, but is mostly interesting because it allows to have a sufficient amount of current flowing through the junction without having to reach a flat band condition. This is required when we want to build field-effect transistors, which consists in a metal-semiconductor-metal structure, the two metals parts are called source and drain, the semiconductor constitutes the channel, where the current is flowing. To have field-effect, a metal-oxide-semiconductor (MOS) junction, a gate, is added above (top gate) or under (back gate) the channel, as shown in Fig. 5. We will here describe a simplified case where we have a uniform semiconductor's doping level.

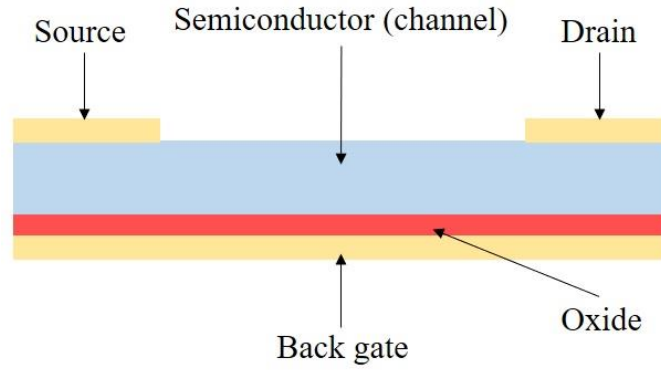


Figure 5: Schematic representation of a back-gated field-effect transistor.

Due to the presence of the oxide, no current is flowing through the gate, creating a MOS capacitance when a voltage is applied to the gate metal. This capacitance allows to modulate the number of carriers injected into the channel through the source and collected at the drain. Applying a voltage on the gate will shift the band in the channel and allow to accumulate carriers ( $V_{gate} < 0$  in p-type SC), or to create a depletion region ( $V_{gate} > 0$ ) or an inversion layer ( $V_{gate} \gg 0$ ) more easily at the M-SC interface.

When we are accumulating holes, the source-drain current  $I_{SD}$  increases, since we are bringing more carriers to be drifted to the drain. In the depletion region, the current drops for several orders of magnitude, creating a large area where no mobile charges can contribute to the current and finally, when we reach a high enough voltage, we are inverting majority carriers at the interface : electrons become majoritarian in a p-type semiconductor and carry the current. Consequently,  $I_{SD}$  increases again with  $V_{gate}$ . Moreover, applying a gate voltage will also vertically shift the energy bands at the metal-semiconductor contact, which consequently modulates the Schottky barrier of the contact and thus facilitate or not the injection of the carriers, as shown in Fig. 6.

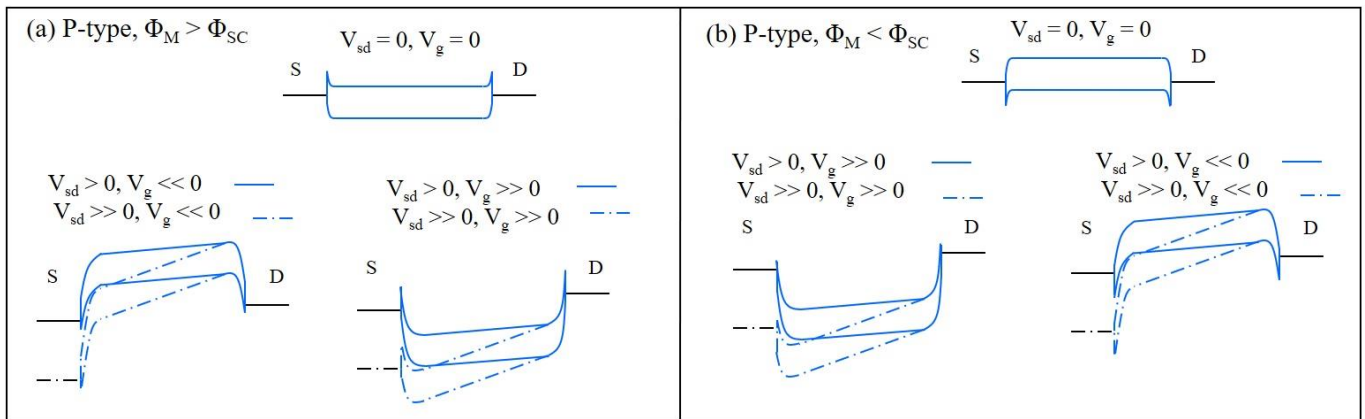


Figure 6 : Band diagram of a field-effect transistor for a p-doped channel with (a)  $\Phi_M > \Phi_{SC}$  and (b)  $\Phi_M < \Phi_{SC}$ . We consider here a long enough channel so that the band bending at the drain is not affected by the voltage applied on the source.

On these band diagrams, we can see that applying a strong negative gate voltage will shift up the band and thus allowing holes to be injected by tunneling through the Schottky barrier (since it is making it thinner) or thermoionic emission. For electrons, it creates a large thermal barrier they can't overcome. When the voltage becomes strongly positive, bands are shifted down and it becomes more and more difficult to inject holes, facing a larger thermal barrier. However, the applied voltage reduces the Schottky barrier width for electron and allows them to be injected in

the channel. Depending on the initial Schottky barrier's height (related to the difference between metal's and semiconductor's work function) of the contact, a really strong positive voltage can be required to make the barrier thin enough to have a good electrons' injection. In this case the ambipolar behaviour of the semiconductor is not symmetric and, for a p-doped semiconductor, we will observe better holes' current modulation rather than the electrons' one. The current at a negative gate voltage is also expected to be higher than at a positive gate voltage since electrons are minority carriers in a p-doped semiconductor. Moreover, considering the effect described above concerning the accumulation or depletion of carriers in the channel enhances this behaviour, regardless of the contacting metal. This is what is generally observed in black-phosphorus based field-effect transistors, some examples will be discussed in the next section of this chapter.

### 1.3 Black phosphorus field-effect transistor

In this section, we will present a brief state of the art concerning black phosphorus field-effect transistors, focusing on the most important investigations concerning transistors' behaviour and the analysis of the contact resistance at the M-SC interface.

Actually, main studies concerning black-phosphorus based field-effect transistors concern the influence of the contacting metal and the thickness of the flake on the transistor's behaviour, unipolar or ambipolar, and the carrier's mobility.

In the literature, most of the studies are based on thin bP flakes, generally thinner than 20 nm, which corresponds roughly to 38 layers. The flake is considered as bulk-like from 5 layers, from the point of view of band structure (Fig 2).

Three different metals are generally used to build these transistors : Titanium (Ti), Nickel (Ni) and Palladium (Pd) and all the reported studies use Silicon Oxide ( $\text{SiO}_2$ ) as back gate dielectric, with various thicknesses.

With these three metals, ambipolar behaviour has been reported, but not in the same conditions. S. Das et al. observed a clear ambipolar behaviour with Ni contacts on flake thicknesses from monolayer to 13 nm (25 layers) with 20 nm  $\text{SiO}_2$  in [5] (Fig. 7 (a)). D. J. Perello et al. observed an ambipolar behaviour with Pd in 14.5 nm (~ 27 layers) and below thick flakes with 300 nm  $\text{SiO}_2$  in [10] (Fig 7 (b)). They also report a transition to an ambipolar p-type dominant conduction as the flake's thickness increases up to ~15 nm (~27 layers). Y. Du et al. observed ambipolar behaviour with both Ni and Pd, but is barely visible with Pd, in their 18.7 nm (~35 layers) thick flake with 90 nm  $\text{SiO}_2$  in [11] (Fig. 7 (c) & (d)). However, Y. Ma et al. have not observed it in a 31 nm thick flake with 300 nm  $\text{SiO}_2$  with both Pd and gold (Au) contacts [12] (Fig. 7 (e) & (f)).

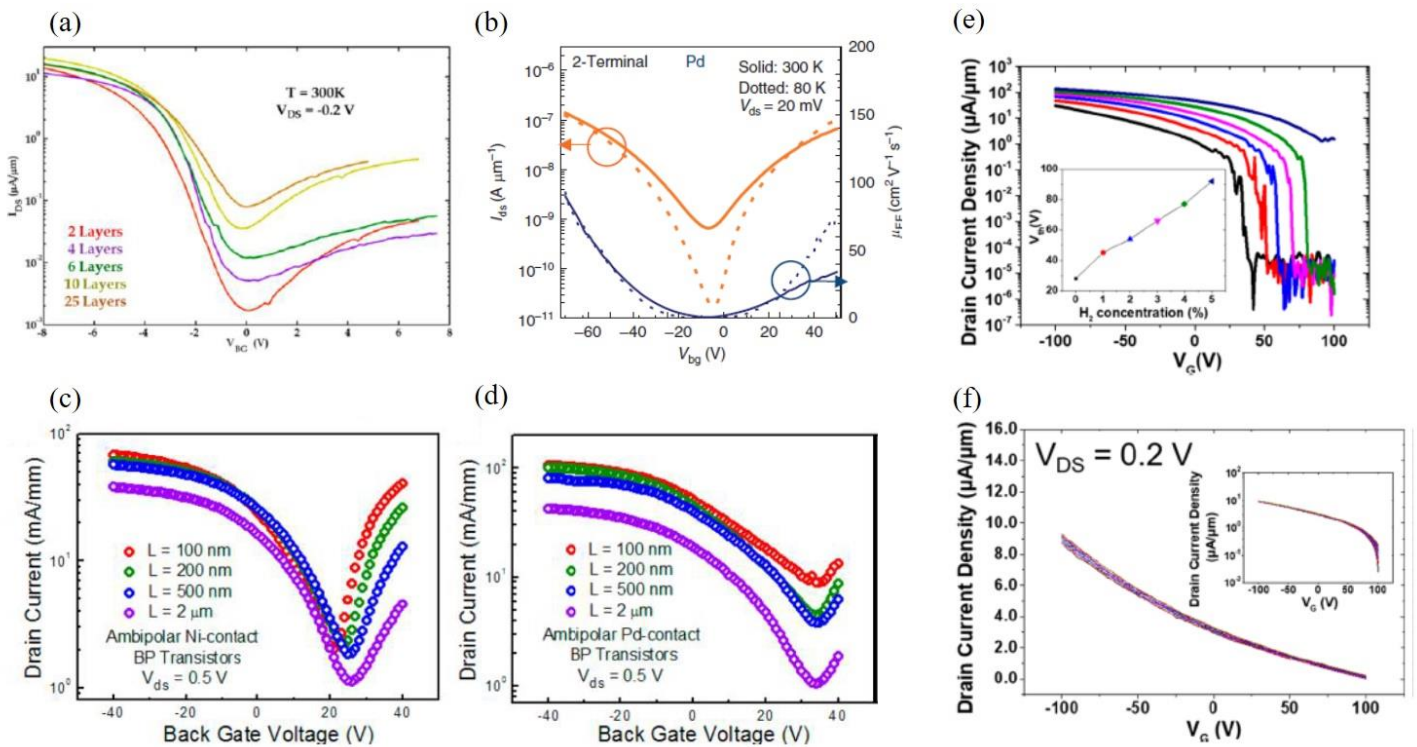


Figure 7 :  $I_{SD}$  vs  $V_g$  characteristics of black phosphorus field-effect transistors at room temperature. (a) Ni contacts, 20 nm  $\text{SiO}_2$  from [5], (b) Pd contacts, 2.5 nm thick flake with 300 nm  $\text{SiO}_2$  from [10], (c) Ni contacts, (d) Pd contacts, 18.7 nm thick flake with 90 nm  $\text{SiO}_2$ , both from [11], (e) black curve Pd contacts, 0%  $\text{H}_2$  and (f) Au contact, ~30 nm thick flake with 300 nm  $\text{SiO}_2$ , both from [12]. The influence of channel length in (c) and (d), along with the temperature behaviour in (b) and the  $\text{H}_2$  concentration dependence in (e) will not be discussed here.

In all of these cases, the dominant conduction is clearly p-type, as shown in Fig 7. These three metals have a high work function ( $\sim 5.0$  eV for Ni,  $\sim 5.4$  eV for Pd, [11] and  $\sim 5.1$  eV for Au [13]), which obviously create an ohmic contact for holes at the M-SC interface since few-layers black phosphorus' work function is reported to be  $\sim 4.5$  eV [1]. This explains the better holes injection and thus the p-type dominant conduction of the transistor. For the Pd contacts, the differences in electron injection behaviour can be attributed to the flake thickness rather than the thickness of the dielectric. The thinner the flake, the better is the ambipolar behaviour. For Ni contacts, a short channel seems to give a better ambipolar behaviour, due to a reduction of the source Schottky barrier width for electrons in a shorter channel with a positive drain-source voltage (or at the drain with a negative source-drain voltage).

Concerning Ti contacts, several cases have also been reported. S. Das et al. [14], H. Liu et al. [15], and D Xang et al. [16] all observed an ambipolar behaviour in their Ti contacted black phosphorus FETs as shown in figure 8.



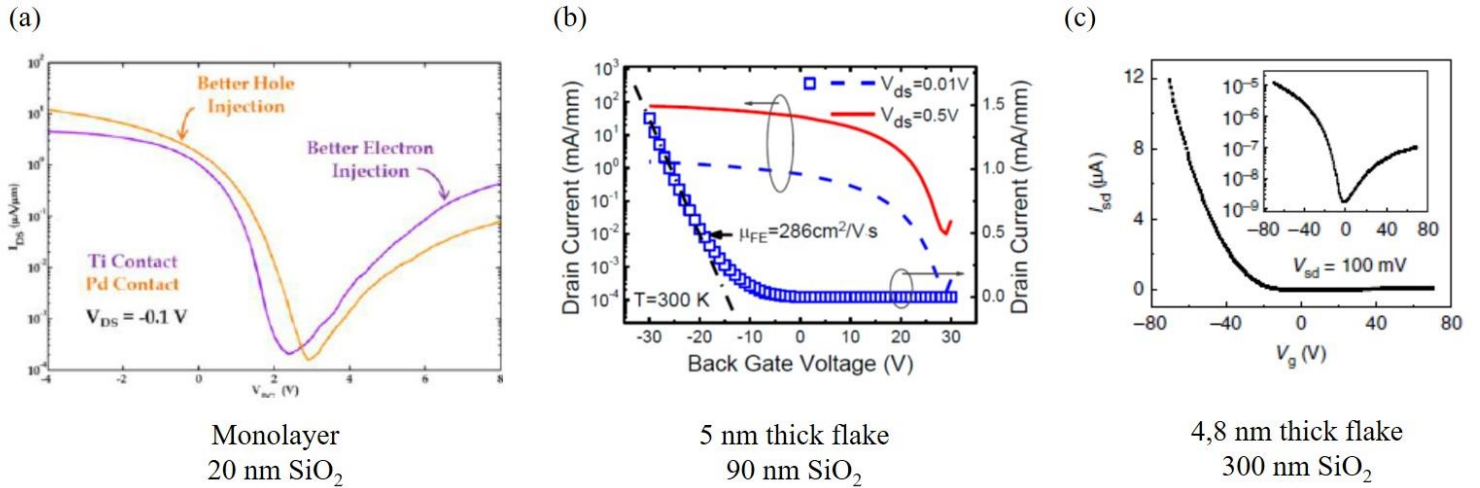


Figure 8:  $I_{SD}$  vs  $V_g$  characteristics of black phosphorus field-effect transistors at room temperature with Ti contacts. (a) from [14], (b) from [15] and (c) from [16]. In (b) arrows indicates the y-axis to follow.

Figure 8 (a) allows us to see that Ti contacts allows a better electrons injection than Pd contacts, due to their lower work function ( $\sim 4.3$  eV [13]) which reduces the drain Schottky barrier height for electrons compared to metals with higher work functions. Consequently, it gives a Schottky M-SC contact as shown in Fig 4, with a Schottky barrier for holes and thus giving a higher contact resistance than in the case of an ohmic contact.

Ambipolar behaviour has also been observed with Chromium (Cr) contacts in a 5 nm thick flake with 90 nm SiO<sub>2</sub> in [7].

One example of dominant n-type conduction black-phosphorus FETs have been reported with Aluminum (Al) contacts by D. J. Perello et al. [10]. This n-type dominant conduction is due to the lower work function of Al ( $\sim 4.0$  eV [10]), which reduces the Schottky barrier height for electrons more than Ti and increases the one of holes.

We can also see in these studies that bP FETs have a good current modulation, with an ON/OFF ratio varying from  $\sim 10^2$  to  $\sim 10^5$ , depending on both thicknesses of the flake and the oxide.

In a few of these works, the contact resistance at the M-SC interface is studied. This is why we propose to investigate it. The most commonly used method is the Transfer Length Method (TLM), which consists in plotting the 2-probes resistance versus the channel length. The equation of the resulting curve is

$$R = \frac{R_s}{W} \times L + 2 \times R_c \quad (1)$$

where  $R$  is the 2-probes resistance in  $\Omega$  (including the contact resistances and the resistance of the channel),  $W$  and  $L$  are the width and the length of the channel in m, respectively, and  $R_s$  and  $R_c$  are the channel and the contact resistance in  $\Omega/\square$  and  $\Omega$  respectively. Since  $R_s$  is in  $\Omega/\square$ , it is in fact a sheet resistance giving the resistance of one sheet of the semiconductor (like if it was 0 thickness).

The intercept at 0-channel length gives twice the single contact resistance, assuming that the contacts are physically the same. This can give a value of the contact resistance at a specific gate voltage or at a given temperature for example and is a good way to compare different contact resistances.

The extraction of the Schottky barrier height of the contact from  $I_{SD}$  vs  $V_g$  characteristics can also be another alternative, with the method depicted by S. Das et al. in [5]. This is interesting if it is not possible to use Arrhenius method, which requires this characteristic at different temperatures. They use the value of the current at the value of  $V_g$  when it leaves the linear regime

in a logarithmic scale, interpreting it as the flat band condition. The thermoionic emission is exponentially related to the Schottky barrier height in energy, and this is the only potential energy carriers have to overcome to be injected at the flat band condition. Thus, at this point, only thermoionic emission is possible and the Schottky barrier can be extracted by modelling this thermoionic current.

They also noticed in [14] that the contact resistance changes with the source-drain voltage (and obviously also with the back gate voltage) and use different assumption depending on the applied voltages to get the source and drain resistance. This will not be discussed here because it should not be of any use for the further analysis in Chapter 3.

Finally, in all of these studies, extracted values for holes' field-effect mobility lie in a range between  $\sim 55 \text{ cm}^2/(\text{V}\cdot\text{s})$  and  $\sim 300 \text{ cm}^2/(\text{V}\cdot\text{s})$ , with the exception of the previously quoted value around  $1000 \text{ cm}^2/(\text{V}\cdot\text{s})$  reported by L.Li et al. [7] in a 10 nm thick flake FET. It is worth to notice that field-effect mobility can be extracted in a 2-probe or 4-probe measurement. 4-probe measurement will give a higher value since it does not take into account effects of contacts. As expected for a layered material, the mobility should vary with the thickness (i.e. the number of layers) due to the interactions between layers. Moreover, since bP is an anisotropic material, the crystalline orientation of the flake directly affects its transport properties. This parameter (the crystalline orientation of the flake with respect to the contacts) is typically not known in the literature about transport measurement in black phosphorus. These two arguments, along with the influence of the contacting metal and the oxidation state of the flake can explain such a scattering in observed values.

From all of these theoretical considerations and observations, we can expect that the nature of the contacting metal on black phosphorus FETs has a real importance, along with the thickness of the flake. This is why it is important, on one hand to investigate on a reproducible way to have thin bP flakes, and on the other hand to have a serious consideration for the contacting metal.

## 2 Sample fabrication process

In this chapter, the process and different technologies we used to build our black phosphorus FETs will be described. We will first focus on black phosphorus' thin flakes exfoliation. Then, methods and steps for field-effect transistors' design and fabrication will be presented, with a brief presentation of two main processes used: Electron Beam Lithography (EBL) and thermal evaporation. NEST laboratory is equipped with a clean room where all of the following process are done.

### 2.1 Black Phosphorus' exfoliation

Actually, mechanical exfoliation with scotch tape is the only reliable method to get proper thin black phosphorus' flakes (for example some chemical exfoliation techniques exist but are known to leave solvent residuals). With this method, long enough flakes with various sizes from 1~10  $\mu\text{m}$  can be obtained. However, this does not allow us to control the thickness of flakes and generally the largest ones are also the thickest ones. Basically, the method consists in stitching the flakes on their substrates.

The substrate we use are made of strongly p-doped Silicon with a thermally grown 300 nm thick silicon dioxide ( $\text{SiO}_2$ ) layer. Before exfoliating, markers and contacting pads are designed on the substrate by negative optical lithography (exposed region will stay after developing), followed by gold evaporation, lift-off and an Oxygen plasma to clean the surface. Exfoliation is done on the  $\text{SiO}_2$  interface.

As said before, black phosphorus is rather reactive with oxygen under light. Thus, we need to exfoliate in a proper atmosphere, since we cannot work in the dark. For this, we use a glove bag, as shown in Fig. 9, in which we constantly flow Nitrogen ( $\text{N}_2$ ) gas.



Figure 9:Glove bag's picture. The bag is filled with nitrogen and we exfoliate black phosphorus inside.



In this glove bag, we prepare the scotch tape used for exfoliation with scratching bulky black phosphorus directly on the tape. Then, we stick the tape with itself and unstick it, several times so that at each time bP' layers are detached. Finally, we stitch our substrate on the tape for one minute. When exfoliation is done, we spin two layers of polymers : a first layer of a copolymer of Methyl-Methacrylate (MMA) with Methacrylic Acid (MAA) (MMA/MAA copolymer) and a second layer of Poly(Methyl-Methacrylate) (PMMA). A 10 minutes annealing at 170°C is realized after each layer to evaporate the solvent in which these molecules are dispersed. These two layers are used here to have a thick resist above exfoliated flakes (~800 nm) to prevent them from oxidizing. Further reasons that explain the use of two different layers will be explained in the next section of this chapter.

## 2.2 Device design

After having exfoliated black phosphorus, we choose the interesting flakes to be contacted based on morphological criteria. Basically, we want flakes with a regular shape and a regular thickness, to have the most homogenous measurements, and as thin as possible. This step consists in looking for them with an optical microscope. The colour of the flake give us an indication on its thickness, and thinnest ones (< 10 nm) are almost transparent. Consequently, it is hard to distinguish them for us from the resist layer. Fig. 10 (a) shows a square into which we look for flakes and (b) the typical kind of flakes we contacted for our study. Now, the real fabrication of the device to be measured begins. It requires several steps that will be described in the following, without entering in the specific details of each process since it is not the purpose of this study.

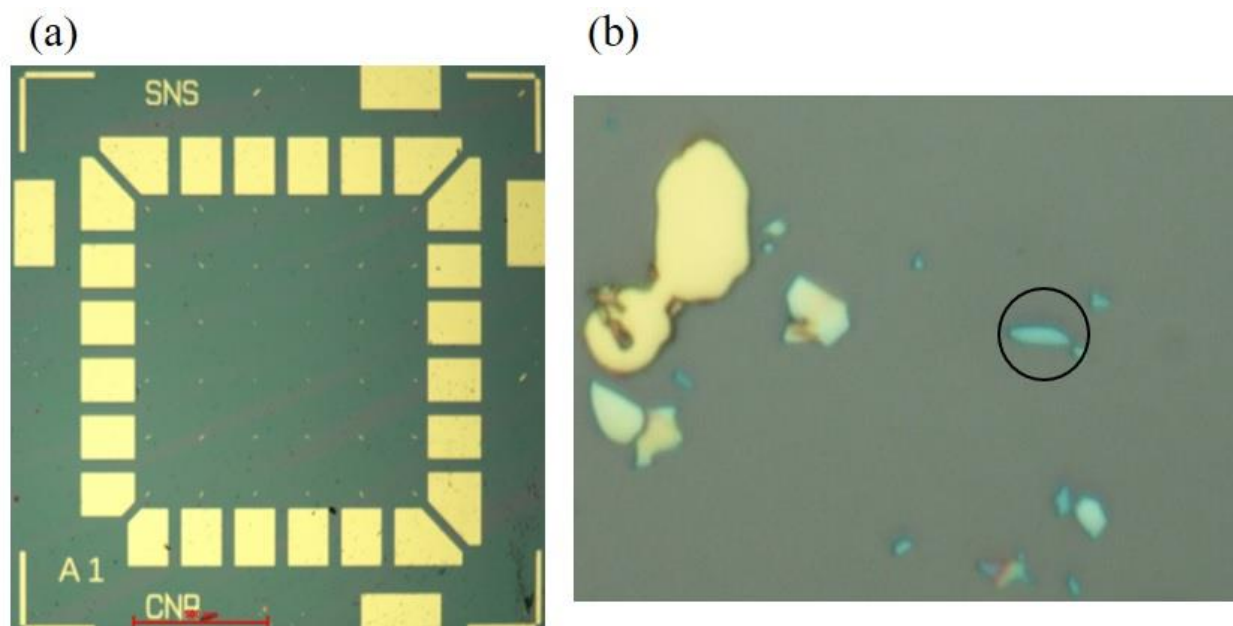


Figure 10: (a) Optical image (5X) of a designed square. Golden pads around are used to build electrical contacts with the flake.

(b) Optical image (100X) of a black phosphorus flake about to be contacted. The length of this flake is around 4  $\mu\text{m}$  and is thicker than 20 nm.

### 2.2.1 Electron Beam Lithography

Once we identified our flakes, we need to design the mask for Electron Beam Lithography. EBL is a lithography process similar to a positive optical lithography in the way that exposed part of the resist will be removed after developing. The difference is that the mask can be freely designed to draw any pattern since the resist will be exposed using an electron beam in a Scanning Electron Microscope (SEM). This technique is mainly used to design fine patterns and is then more adjustable, but also requires much longer exposing times respect to photolithography, proportional to area to be exposed. The current of the electron beam and the dose (charge per unit of area) are critical parameters. For example, a large aperture (or high current) will give a lower resolution, but will allow us to expose large areas faster, generally where the best resolution is not required.

The dose corresponds to the amount of exposure in the area of the beam. The higher is the dose, the more polymer chains will be broken in that area of resist.

The current is fixed for a given value of aperture and voltage applied to the electrons and allows us to know the time it will take to expose a given area (at the same dose, it will take less time with a higher current).

Our bilayer of resist is formed by an upper layer of PMMA and a lower one of MMA/MAA copolymer (called MMA from now on for simplicity). Since PMMA is the polymer of MMA, it has a higher mass per unit of volume, and hence requires a higher dose to be exposed with EBL. Exposing the resist to an electron beam will break long polymer atomic chains and allow them to be solved in a proper solvent, which will not solve longer chains. To avoid giving too much time of exposure to our sample, we then spin a first layer of MMA and then PMMA. We will also discuss later in this section another advantage concerning the spinning of these two layers for development of the resist.

Typically, a high electron acceleration voltage, between 20-30 kV, is used to reduce scattering effects, what allows us to have a sharp shape for the exposed area since backscattered electrons are those which break the polymer chain.

In our case, we decided to design a matrix of parallel rectangular shaped contacts of 200 nm width, spaced at least by 400 nm. The width of the contact is quite thin so that we can have at least four of them on a  $\sim 3 \mu\text{m}$  long flake. Thus, during the EBL, a small aperture (10  $\mu\text{m}$ ) and a 400  $\mu\text{C}/\text{cm}^2$  dose are used to expose these contacts on the flake. With these parameters, we have a good resolution on the exposure of the contact and the dose is sufficient to expose properly our resist bilayer.

We also draw a wider path between these contacts and the large gold pads (those shown in Fig 10 (a)), that will be exposed with the same dose but a bigger aperture, 30  $\mu\text{m}$  for those which are touching the contacts on the flake and 60  $\mu\text{m}$  for farer and bigger ones. An example of typical designed EBL masked is given in Fig 11.

The next step is to develop the resist. By putting the sample into the specific solvent for PMMA, the exposed part will be removed from the sample, letting  $\text{SiO}_2$  and the flake naked on the designed path. The solvent we use is a mixture of MIBK (Methyl isobutyl ketone) and isopropanol with 1:3 ratio (AR600-56 is its commercial name). We put our sample into it for two minutes and then into isopropanol for few seconds, which will stop the development. Once the sample is out of the isopropanol's beaker, we flush nitrogen to dry it. During this step, the behaviour of our two layers of resist is interesting because, since MMA has been a bit overexposed, it will be also a bit overdeveloped. Thus, the shape of the hole will be really sharp

on the PMMA layer, and smoother and larger on the MMA layer, what will allow us to have a better metal deposition for the contacts and easier lift-off.

After the development, we realize a quick O<sub>2</sub> plasma to clean the exposed surface of the sample and so, to have a better metal stitching on the contact area. After taking out the flake from isopropanol, the flake is exposed to air. Hence, we have to be really fast to put it into the ion etching chamber, and the same after this to put it into the thermal evaporator chamber, in order to reduce the oxidation as much as possible.

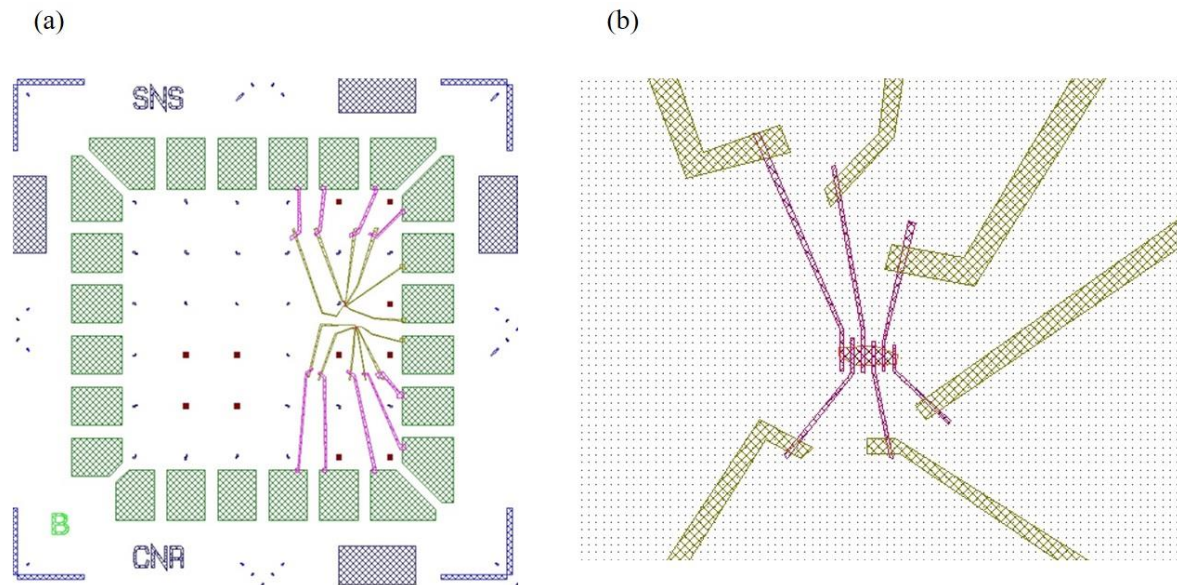


Figure 11 : EBL mask designed for the square (a) and the flake (b) from Fig 10.

### 2.2.2 Thermal evaporation

The following step of the fabrication is the thermal evaporation of the contacting metal. The evaporator is made of a vacuum chamber, a sample holder on the top protected by a removable shutter and four boats in the bottom of the chamber, one for each metal the evaporator is made for (Ni, Au, Ti or Cr, and Ge/Au for our evaporator). Metals can either be rods or little pieces that we put into a tungsten crucible. To evaporate, we heat the metal by applying a current to the crucible or to the rod. The intensity of the current, and thus the heating temperature, depends on the melting point of the metal. Procedures for each metals are computer assisted. Moreover, the evaporator is equipped with a rotating carousel to move the sample on the top of the selected metal crucible/rod.

The evaporation is performed under a good vacuum of  $10^{-6}$  mbar. To reach this value in our evaporator, we evaporate chromium, for the getter effect, keeping the shutter closed in front of the sample, until the pressure stops decreasing. Once the pressure is stable, we stop evaporating chromium. Then, we evaporate 10 nm of our contacting metal (Cr, Ni or Ti) and 100 nm of gold on our sample. Thanks to the hole we created with our development, we should have sharp edges for our contacts, the evaporated metal “beam” being guided by the sharp shape of the hole in the top of the resist layer (PMMA). The smoother and larger hole in the MMA part of the resist (closer to the sample) allows us to have a homogenous height of the metal deposition, without accumulating metal on the edges.

After the evaporation, the sample is fully covered with gold. We proceed with a lift-off to keep only the designed contacts. We put the sample in a beaker of acetone at 50°C for 15 min.

This will remove all the PMMA and MMA layers of the sample, with the metal deposited on it so that it leaves only the designed metallic contacts. Then we spin again two layers of resist to protect the sample from air. Fig 12 shows a contacted black phosphorus flake.

(a)

(b)

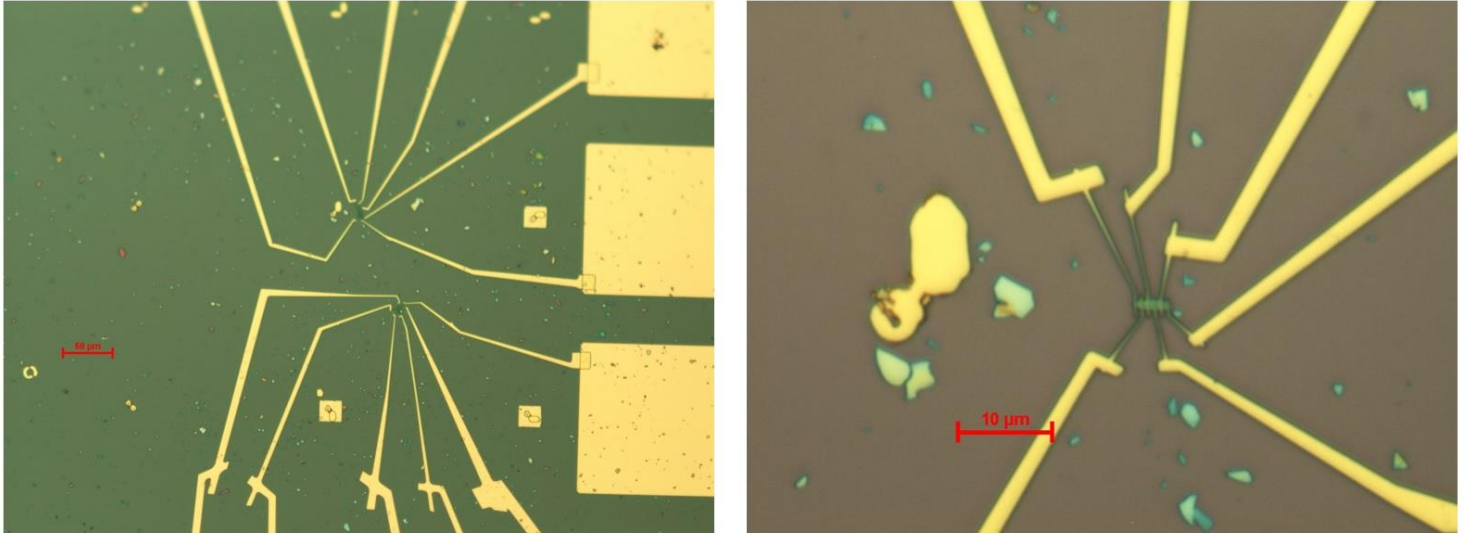


Figure 12 : Optical images of contacted devices. (a) is 20X magnification, the scale bar represents 50  $\mu\text{m}$ . (b) 100X magnification of the top device of (a).

Since we spun a second layer of resist, we need to open holes on the contact gold pads for bonding (like those shown in Fig 12 (a)). Thus, we proceed with a second EBL step in which we only expose pads, followed by the same development previously described.

Finally, we then glue the sample with silver paint on a 16-pins dual in-line chip carrier (to get an electrical contact between the conductive back of the dual in-line and the p-doped Si part of the substrate, which is our back gate).

The last step consists in making an electrical contact between the gold bonding pads of the sample to the contacts of the dual in-line with gold wires. For this, we use a wire bonder involving a needle on which the gold wire is fixed, as shown in Fig 13. Using an optical microscope, we bring the needle where we want to stitch the wire on the contact on the dual in-line and the wire is locally melted through an ultrasonic pulse sent through the needle. Then we move the needle to the sample and stitch it the same way. Once this is done for each contact and the back gate, the sample is ready to be set up in the installation we use for transport measurement that will be presented in the next chapter.

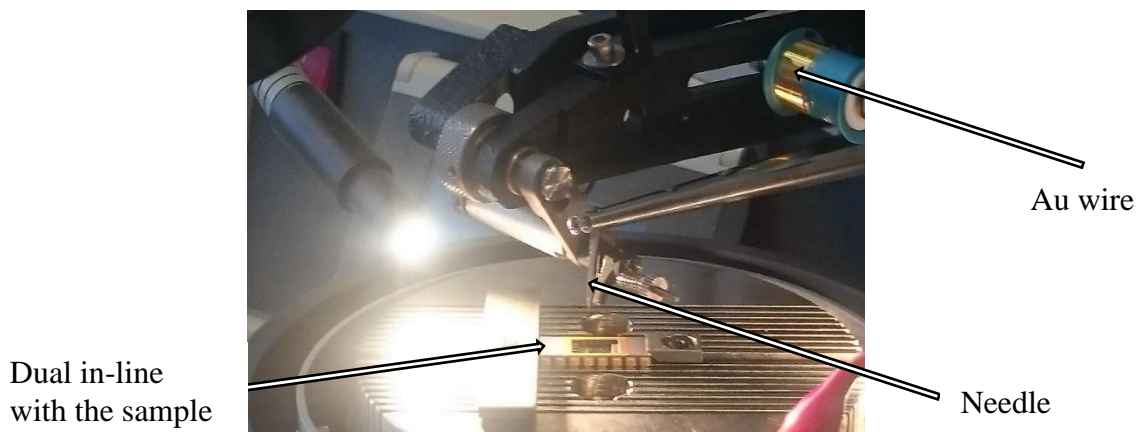


Figure 13: Picture of the bonder showing the needle with Au wire

## 3 Measurements and analysis

In this chapter, results obtained concerning the contact resistance and the behaviour of the different devices depending on the contacting metal will be presented. The first section will present the experimental setup we used to perform measurements and the second and third section will focus on the obtained results.

### 3.1 Experimental setup

The setup in which the bP FETs are measured is made of a dipstick in which we put the sample. This is basically a tube that can be pumped through a valve on one side and with a sample holder on the other side. It is also equipped with a diode for temperature measurement, placed right behind the sample holder. The electrical connections pass through the tube and are connected to a box with LEMO connectors with a Fischer cable. Each pin of the dual in-line has an output on the box and a switch that allows us to ground the pin or make it floating. The box is mounted in a rack with measurement instruments and power supplies.

For room temperature measurements, the dipstick is just pumped with a turbo-pump so that we reach a vacuum of the order of  $10^{-5}$  mbar. We pump over our sample because of the reactivity of black phosphorus with oxygen that could be increased when a current is flowing through the device. We generally perform measurements in dynamic vacuum.

For low temperature measurements, the dipstick is pumped a bit longer to reach a vacuum in the order of  $10^{-6}$  mbar. The pumping system is then disconnected and we put the dipstick in a cryostat allowing us to reach liquid Helium temperature ( $\sim 4.2$  K). In the following, low temperature means liquid Helium temperature.

To measure bP FETs, different measuring instruments are used. They can all be monitored with a homemade LabView program.

Concerning current versus voltage I-V characteristics from which we get the 2-probes resistance of our device, we use the DC output channel of a Lock-In Amplifier as a voltage source to apply a voltage between 1 mV and -1 mV. The induced current is measured with a current preamplifier and a multimeter.

For 4-probe measurements, we use two Lock-In Amplifiers. One is used to apply an alternating (AC) current of 100 nA between the source and the drain with a 17 Hz frequency (this low value should not create a big difference with the DC 2-probe measurements) and measure the current flowing in the device from the drain contact. The second Lock-In Amplifier is used to measure the voltage between two inner contacts of the device.

These two different ways of measuring the device's resistance are used to get the contact resistance. From the I-V curves taken at different channel lengths, we can extract the contact resistance using the Transfer Length Method (TLM) (cf Chapter 1). We can also have an evaluation of the contact resistance by subtracting the 4-probe resistance from the 2-probe value.

We also measure the source-drain current ( $I_{SD}$ ) versus back gate voltage ( $V_g$ ) from which we can theoretically extract the field-effect mobility ( $\mu_{FE}$ ) and the Schottky barrier's height, as explained in Chapter 1. To perform these measurements, we use a Lock-In Amplifier to apply the source-drain voltage ( $V_{SD}$ ) and to measure the source-drain current  $I_{SD}$ . The back gate voltage is a DC bias applied with a Keithley 2600 between -50 V and 50 V at room temperature and between -80 V and 80 V at low temperature. In the same range, we also measure the 4-probe resistance



versus back gate voltage to have a different estimation of the field-effect mobility without complications induced by contacts.

Finally, we also measured I-V curves in a wider range (-100 mV to 100 mV) at different back gate voltages to see if the contact keeps an ohmic behaviour in a wider range. For these measurements, we use the Keithley 2600 to apply the source-drain voltage and the back gate voltage. The current is measured both with the Keithley (which allows to apply and measure on the same channel) and with the preamplifier and the multimeter.

### 3.2 Electrical contact engineering

In this section, we will mainly focus on the analysis of the I-V curves, to get TLM graphs, and on the comparison with the 4-probe measurements. The extraction of the Schottky barrier height from the  $I_{SD}$  vs  $V_g$  curves can also be a good parameter to evaluate the contact resistance but as we will see in the next section, the shape of our curves does not allow us to get this information.

We will here compare results obtained with three different contacting metals : Chromium, Nickel and Titanium.

Figure 14 shows the I-V curves measured on three different devices, one with Chromium contacts, one with Titanium contacts and one with Nickel contacts.

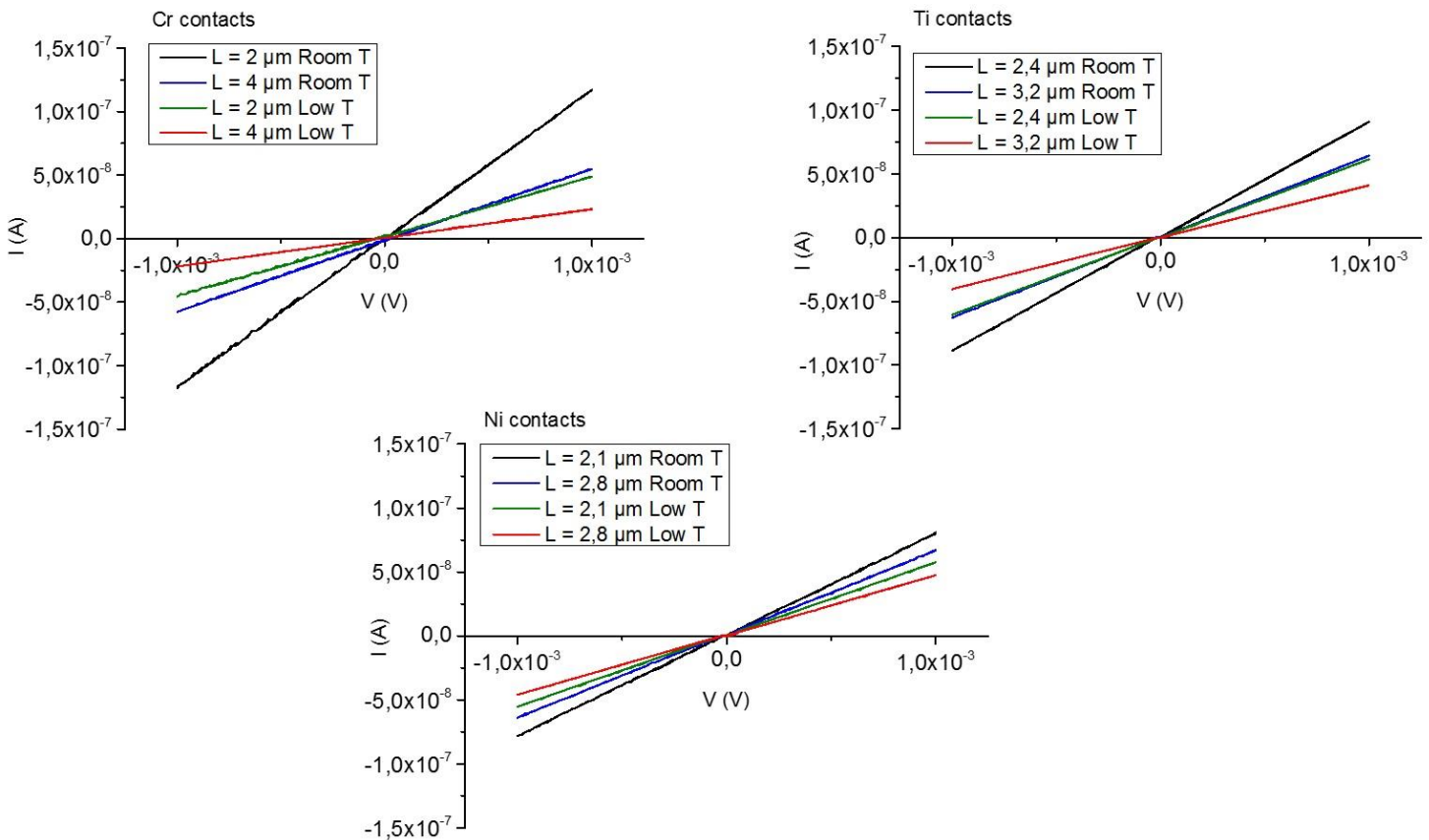


Figure 14: I-V curves for three different devices with Chromium, Titanium and Nickel contacts.

We can here see that all of these I-V curves are linear between 1 mV and -1 mV, which is a quite small applied voltage. Thus, no matter the contacting metal, all the devices display an ohmic-like contact at the interface with black phosphorus in this voltage range. This is interesting for us since an ohmic contact allows an easier carrier injection than a Schottky contact. Nevertheless, in this range, we cannot tell if the contact is really ohmic or not because even a Schottky contact could display a linear shape close to 0 V applied. From the theory described in Chapter 1, we can expect the Nickel and Chromium contacts to be ohmic because their work function is superior or equal to the one of black phosphorus ( $\Phi_{\text{Ni}} \approx 5.0$  eV [11],  $\Phi_{\text{Cr}} \approx 4.5$  eV [17],  $\Phi_{\text{bP}} \approx 4.5$  eV [1]). On the contrary, we can expect the contact to be Schottky with Titanium since its work function is lower than 4.5 eV ( $\Phi_{\text{Ti}} \approx 4.3$  eV [13]).

The value of the 2-probe resistance can be extracted from these curves by inverting the value of the slope. Thus, the higher the slope the lower is the resistance. We can see that the resistance increases with the length of the channel, as expected from the relation between resistance and resistivity :

$$R = \rho \frac{l}{S} \quad (2)$$

where  $\rho$  is the resistivity in  $\Omega \cdot \text{m}$ ,  $l$  the length of the channel in m and  $S$  the cross-section (width times thickness) of the channel in  $\text{m}^2$ .

We can also note that the resistance increases at low temperature. When the temperature decreases, less carriers are thermally excited. Therefore, the valence band is less filled and less holes contribute to the conduction. However, the hole mobility increases at low temperature since there is less scattering elements, increasing the carriers velocity and hence the current. There is then a competition between increase of the mobility and decrease of the number of carriers. In black phosphorus, the increase of the mobility does not seem to be able to dominate the emptying of the valence band. Consequently, the current decreases and the resistance of the channel increases at low temperature.

We do not compare quantitatively these three devices together because they have different geometry, they were not fabricated at the same time and the used black phosphorus was not exfoliated in the same way. Thus, a proper quantitative analysis would require working with the resistivity and not the resistance, but we cannot calculate it because we do not know the thickness of our sample (it would require an Atomic Force Microscopy but doing this with bP in the air means destroying the devices).

These 2-probe resistance measurements include the resistance of the channel. From these curves, we can then build a Transfer Length Method (TLM) graph, corresponding to the 2-probe resistance versus the channel length. This allows us to extract the contact resistance at the intercept at 0 channel length. A first TLM graph is shown in figure 15 (a), for the Chromium sample we study here (the same as in figure 14). This flake is a bit particular since its thickness is not uniform, as can be seen in figure 15 (b). The yellowish part is thicker than the blueish part and the measured resistances on these two part are different. We will therefore study them as two different flakes.

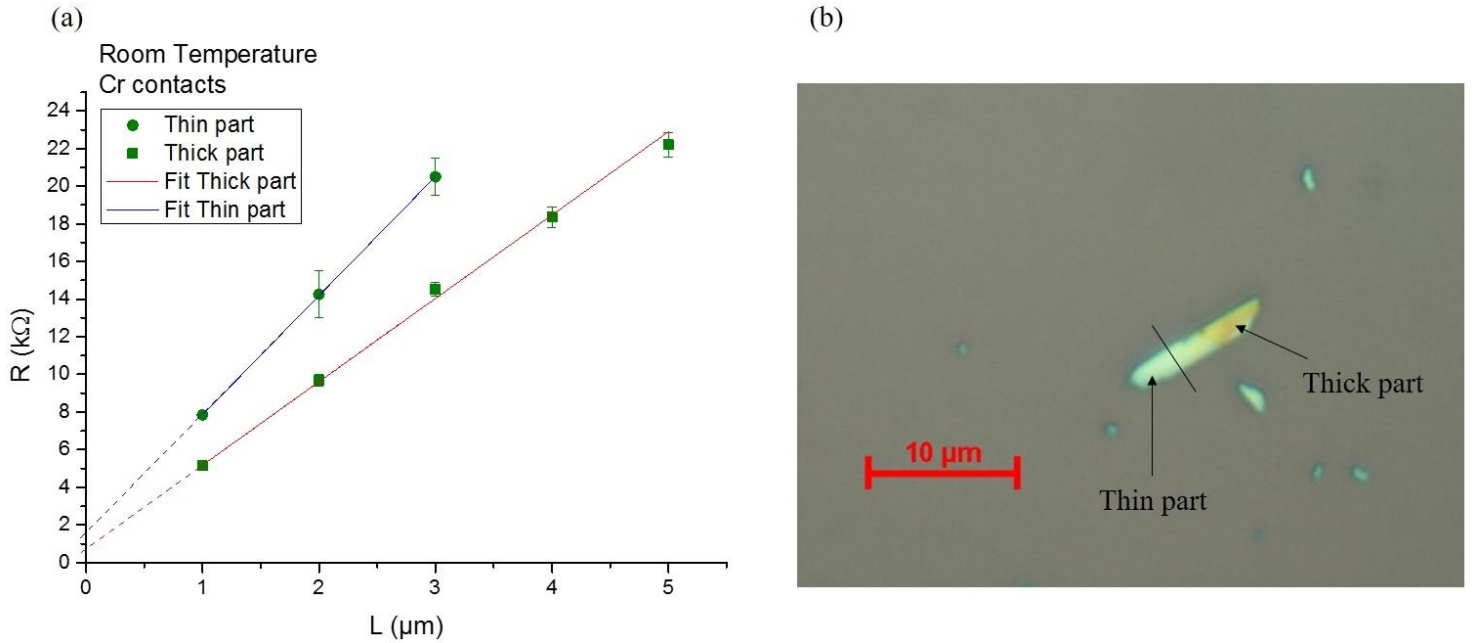


Figure 15: (a) TLM graph for the thick and the thin part of the chromium device at room temperature. Dashed lines are a guide to the eye. (b) Optical microscopy image of the black phosphorus flake where we can see the two different thicknesses.

We can see that the thinner part shows a higher resistance than the thicker part, as expected from equation (2). Results of the fitting are shown in table 1.

Table 1 : Fitting results of the two curves of figure 15 (a) at room temperature.  $R_s$  is the channel resistance,  $W$  the width of the channel,  $R_c$  the contact resistance (half of the intercept with 0) and  $L_T$  is the transfer length.

Thick part					
Equation Fit	$R_s/W$ ( $k\Omega/\mu m$ )	$R_s$ ( $k\Omega/\square$ )	$R_c$ ( $k\Omega$ )	$\rho_c$ ( $k\Omega.\mu m^2$ )	$L_T$ ( $\mu m$ )
		$W = 2 \mu m$			
$R = 4,43L + 0,75$	$4,43 \pm 0,11$	8.86	$0,38 \pm 0,12$	0.15	0,13
Thin part					
Equation Fit	$R_s/W$ ( $k\Omega/\mu m$ )	$R_s$ ( $k\Omega/\square$ )	$R_c$ ( $k\Omega$ )	$\rho_c$ ( $k\Omega.\mu m^2$ )	$L_T$ ( $\mu m$ )
		$W = 2 \mu m$			
$R = 6,34L + 1,52$	$6,34 \pm 0,03$	12.68	$0,76 \pm 0,15$	0.30	0,15

To compare the contacts, we use the contact resistivity, which is calculated by multiplying the contact resistance with the area of the contact ( $0.2 \mu m \times W$ ), in order to get a better comparison between flakes of different shape. It is a 2D resistivity independent of the flake thickness, while the channel (or sheet) resistivity  $\rho_s$  is a volume resistivity that cannot be calculated without the flake thickness.

The channel resistance  $R_s$  increases by around 45 % between the thick part and the thin part. The contact resistivity  $\rho_c$  increases as well, but by a factor 2. This means that the thickness of the black phosphorus under the contact has an influence on the value of the contact resistance. However, increase in  $\rho_c$  is higher than increase in  $R_s$ . This implies that there must be another contribution to this increase.

Another effect can contribute to increase the contact resistance, known as current crowding. This is quantified with the transfer length, which represents the average length travelled by the current carriers in the semiconductor below the contact. When this transfer length is lower than the contact width, we are in current crowding conditions and this means that the carriers are not



uniformly injected along the contact but on its edges, as shown in figure 16. Carriers may be scattered in this part of the contact and thus the resistance of the contact would be increased in these conditions.

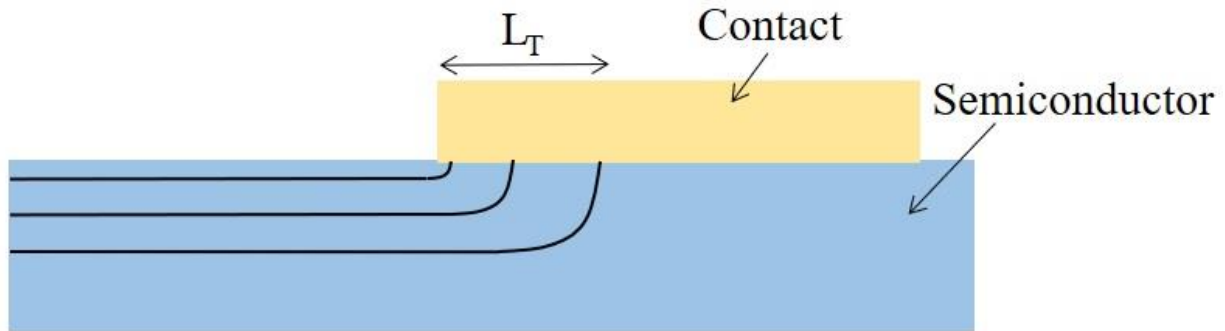


Figure 16 : Schematic sketch of current crowding. If the transfer length  $L_T$  is small, the carriers travel more in the contact than in the semiconductor.

The transfer length can be evaluated with transmission line model :

$$L_T = \sqrt{\frac{\rho_c}{R_s}} \quad (3)$$

where  $R_s$  is the channel sheet resistance in  $\Omega/\square$  and  $\rho_c$  the contact resistivity in  $\Omega.m^2$ , calculated as the contact resistance times the area of the contact.

The transfer lengths of the thick part and the thin part are  $L_T = 0.13 \mu m$  and  $L_T = 0.15 \mu m$ , respectively, which is lower than the width of our contacts ( $0.20 \mu m$ ). Therefore, we are in current crowding conditions on both parts of the flake. The thick part seems to be a bit more concerned than the thin part (since its transfer length is lower). This means that, relatively to the channel sheet resistance, the contact is more resistive in the thick part. However, the contact resistivity of the thick part is lower than the one of the thin part ( $\rho_{c|thick} = 0.15 \text{ k}\Omega.\mu m^2 < \rho_{c|thin} = 0.30 \text{ k}\Omega.\mu m^2$ ). Thus, this cannot explain the superior increase of the contact resistance in the thin part.

This other contribution to the increase of the contact resistance can also be attributed to a superior oxidation state of the thinner part. Black phosphorus is known to be more reactive in few-layer form than in bulk form [18]. However, as we just saw, this cannot be quantified with a current crowding evaluation.

Figure 17 shows TLM graphs for the same devices as figure 14 and results of the fitting are shown in Table 2. Concerning the Chromium sample, only the thick part will be treated here in order to not overload the graphs.

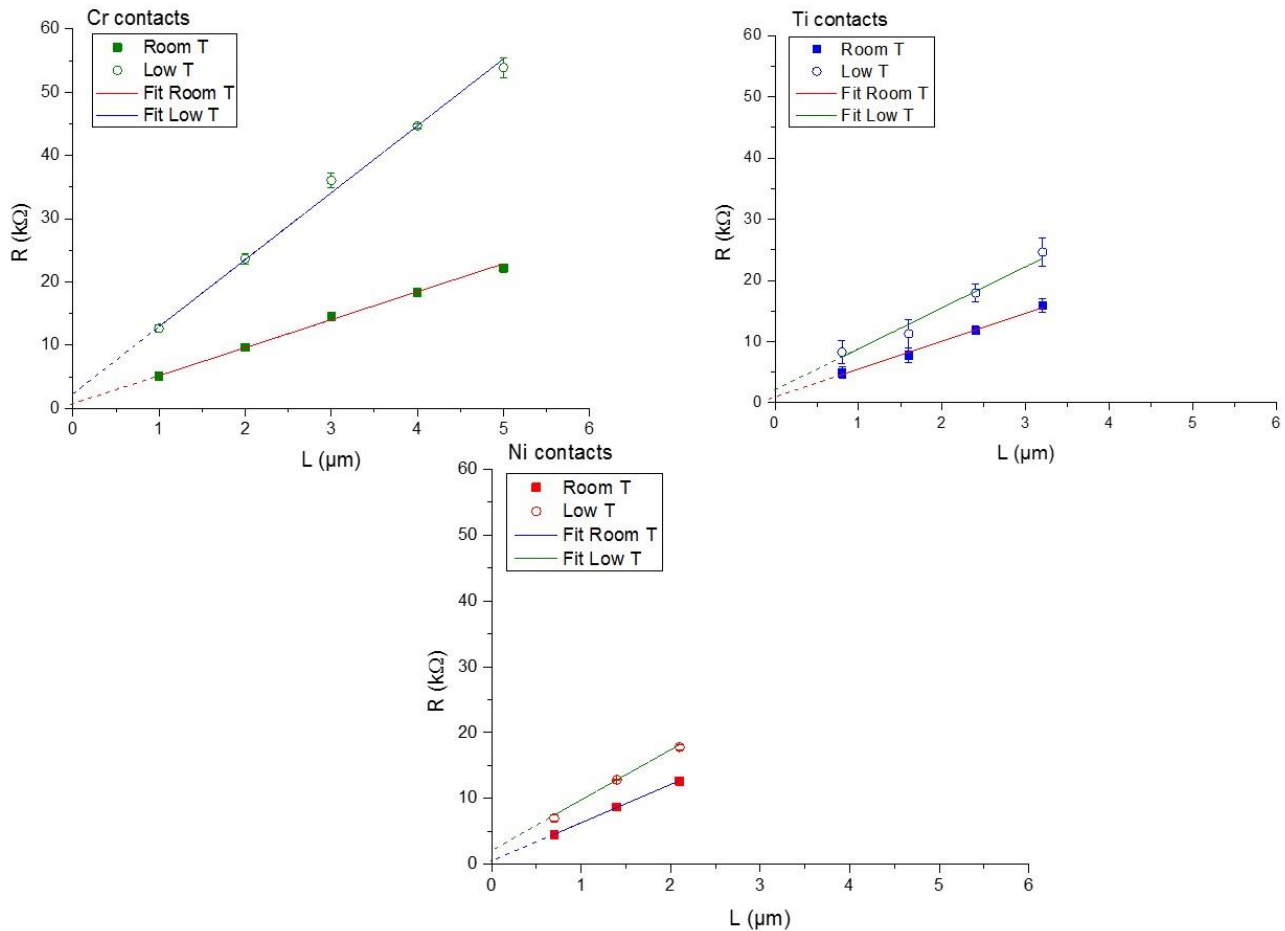


Figure 17: TLM graphs of the three samples with Chromium, Titanium and Nickel contacts. Dashed lines are used as a guide to the eye.

Each point is here affected with an error bar (as well as in figure 15 (a)), which are taken into account in the fitting to get the contact resistance. With the geometry we chose to build for our devices (figures 11 (b) and 12 (b)), we can measure several times a same channel length, but in different parts of the flake. This creates a scattering in the measured resistance for one channel length, mostly due to the non-uniform geometry. We can then calculate a standard deviation of the value of the resistance for each point. However, for the longest value of channel length, which means the furthest contacts on each flake, we can only have one measurement (we could have repeated several time the measurement for these length between the same contacts but it would have given us a statistical scattering instead of a physical scattering that we cannot merge). To calculate a standard deviation for this point, the average of all the standard deviation of the same flake is calculated. But, to get a physically acceptable fitting, the number of measurements needs to be taken into account. We then calculate the standard error, which is the standard deviation divided by the square root of the number of measurements. The fitting is then calculated with a weight, inversely proportional to the square of the standard error (proportional to the number of measurement). Thereby, a point will have more weight if it has more measurements, but also if its error is small.

Table 2: Fitting results of the TLM graphs from figure 16.  $R_s$  is the channel resistance,  $W$  the width of the channel,  $R_c$  the contact resistance (half of the intercept with 0) and  $L_T$  is the transfer length.

Room Temperature							
	Equation Fit	$R_s/W$ (k $\Omega/\mu\text{m}$ )	$R_s$ (k $\Omega/\square$ )	$R_c$ (k $\Omega$ )	$\rho_c$ (k $\Omega.\mu\text{m}^2$ )	$L_T$ ( $\mu\text{m}$ )	$R_c$ from 4-probe measurements (k $\Omega$ )
			$W = 2 \mu\text{m}$				
Cr	$4,43x + 0,75$	$4,43 \pm 0,11$	8.86	$0,38 \pm 0,12$	0.15	0,13	$0,28 \pm 0,08$
			$W = 1.3 \mu\text{m}$				
Ti	$4,56x + 0,97$	$4,56 \pm 0,23$	5.93	$0,49 \pm 0,25$	0.13	0,15	$0,47 \pm 0,05$
			$W = 0.9 \mu\text{m}$				
Ni	$5,83x + 0,48$	$5,83 \pm 0,11$	5.25	$0,24 \pm 0,07$	0.04	0,09	$0,15 \pm 0,01$
Low Temperature							
	Equation Fit	$R_s/W$ (k $\Omega/\mu\text{m}$ )	$R_s$ (k $\Omega/\square$ )	$R_c$ (k $\Omega$ )	$\rho_c$ (k $\Omega.\mu\text{m}^2$ )	$L_T$ ( $\mu\text{m}$ )	$R_c$ from 4-probe measurements (k $\Omega$ )
			$W = 2 \mu\text{m}$				
Cr	$10,59x + 2,35$	$10,59 \pm 0,22$	21.20	$1,18 \pm 0,40$	0.47	0,15	$1,17 \pm 0,39$
			$W = 1.3 \mu\text{m}$				
Ti	$6,72x + 2,09$	$6,72 \pm 0,74$	8.75	$1,05 \pm 0,80$	0.27	0,18	$1,0 \pm 0,5$
			$W = 0.9 \mu\text{m}$				
Ni	$7,63x + 2,15$	$7,63 \pm 0,61$	6.87	$1,08 \pm 0,43$	0.19	0,17	$0,97 \pm 0,15$

At room temperature, we can see that, as expected from the theory described in Chapter 1, titanium contacts are more resistive than the nickel one, since titanium's work function is closer to the conduction band than the nickel one (and black phosphorus is a p-type semiconductor). With titanium, holes have to overcome the Schottky barrier created by the Fermi level alignment (cf figure 4). As we previously saw, this could also be explained by the values of the found channel sheet resistance  $R_s$  since the titanium device is more resistive than the nickel one ( $R_{s|Ni} = 5.25 \text{ k}\Omega/\square < R_{s|Ti} = 5.93 \text{ k}\Omega/\square$  at room temperature). However, the increase between contact resistivity is more important (325 %) than the increase between channel resistance (13 %). Current crowding cannot explain as well the difference between contact resistivity since it appears that this effect is more pronounced with nickel contacts ( $L_{T|Ni} = 0.09 \mu\text{m} < L_{T|Ti} = 0.15 \mu\text{m}$ ). If nor current crowding, nor the flake resistance can explain the difference between contact resistivity, then the work function of the metal is the parameter ruling the contact behaviour.

Concerning the sample with chromium contacts, the measured contact resistivity is higher than the one of titanium and nickel. This result is surprising if we consider the theory described in Chapter 1 since chromium has a higher work function than titanium. Then, if we just consider a carrier injection point of view, chromium contacts should give a lower contact resistivity. However, in this case, the black phosphorus of the chromium device is more resistive than the one of the titanium device ( $R_{s|Cr} = 8.86 \text{ }\Omega/\square > R_{s|Ti} = 5.93 \text{ }\Omega/\square$  at room temperature). As we saw previously, the black phosphorus beneath the contact has an influence on the contact resistance. Thus, here, the higher contact resistivity value can be explain by the fact that the resistance of the black phosphorus beneath the contact is higher. The current crowding evaluation with the transfer length also goes in this way here, showing a bit more current crowding in the case of chromium contacts ( $L_{T|Cr} = 0.13 \mu\text{m} < L_{T|Ti} = 0.15 \mu\text{m}$ ).

The sample with nickel contacts also shows a small transfer length meaning that we have more current crowding for this kind of contacts. However, the contact resistivity with the nickel contacts is here the smallest, meaning that current crowding is not the key factor to understand mechanisms that contributes to the contact resistivity. This proves us that a metal with a high work function, like nickel ( $\Phi_{\text{Ni}} \sim 5 \text{ eV} > \Phi_{\text{bP}} \sim 4.5 \text{ eV}$ ) gives an ohmic contact with a lower resistivity than a Schottky contact, like we have with titanium ( $\Phi_{\text{Ti}} \sim 4.3 \text{ eV} < \Phi_{\text{bP}} \sim 4.5 \text{ eV}$ ).

At low temperature, we observe the same trend in the results. The measured channel and contact resistances are higher than those at room temperature, as expected since a semiconductor's resistivity increases with decreasing the temperature because of carrier freezing.

We can also note that low temperature tends to decrease the current crowding effect (all the transfer length are higher at low temperature than at room temperature). This can be explain by the fact that the mobility of black phosphorus increases at low temperature (see next section) and thus the transport becomes more ballistic in the semiconductor. Thus, current carriers prefer travel in the semiconductor than in the contact.

We can also see that contact resistances extracted from the comparison between the 4-probe and 2-probe measurements ( $R_{4\text{-probe}} - R_{2\text{-probe}} = 2 \times R_c$ ), are in good agreement with those extracted from the TLM method, for both room and low temperature, as a further proof of the strength of our estimation.

Finally, we can see that the error on the contact resistance with titanium contacts is higher than for nickel and chromium contacts (it can also be seen with the error bars' size on figure 16). Even if those samples were not fabricated in the same time, we can assume that the oxidation state of black phosphorus was not really different between this three samples (bulk bP used for exfoliation is kept in dark and under vacuum). This shows us that titanium deposition is not as good as chromium and nickel and some titanium oxide ( $\text{TiO}_2$ ) might be deposited. On titanium-contacted flakes, some contacts were completely insulating without any reason (knowing that for one flake, the process is exactly the same for all contacts). From this, we can state that this could be a good reason not to use this metal to build contact on bP.

Another parameter that could have an importance in the measured sheet resistance and contact resistance is the crystallographic orientation of the flake. Since black phosphorus is an anisotropic material, it also displays anisotropy in its properties. Depending on the armchair or zigzag direction, the resistance of the flake is different and we do not know this orientation for our contacted flakes.

Giving the best contacting metal to black phosphorus would here be a bit vain. It obviously depends on what we want to do with our bP FET, as we saw in the state of the art in Chapter 1. Still, we can state something from the contact resistance point of view. From these results, nickel appears to be the best candidate, giving the lowest contact resistivity among the three tested metals. This can be explained by the pure ohmic contact it creates with black phosphorus, according to the theory described in Chapter 1. To confirm this, some further measurements of I-V curves in a wider range were done but results are still under analysis. From the shape of these curves we can see if the contact remains ohmic or not in a wider range and a fitting process can be done to try to extract the Schottky barrier's height value.

In our case titanium seems to be the one to avoid due to the difficulty we had to deposit it properly, hence affected resistances measurements. We can also state that current crowding does not seem to be a major effect contributing to the contact resistance.

### 3.3 Transport measurements as a function of gate voltage

In this section, we will focus on the analysis of source-drain current versus back gate voltage characteristics that allows us to see if we have an ambipolar behaviour and to extract the field-effect mobility.

Figure 18 shows the  $I_{SD}$  versus back gate voltage for our three samples at both room and low temperature.

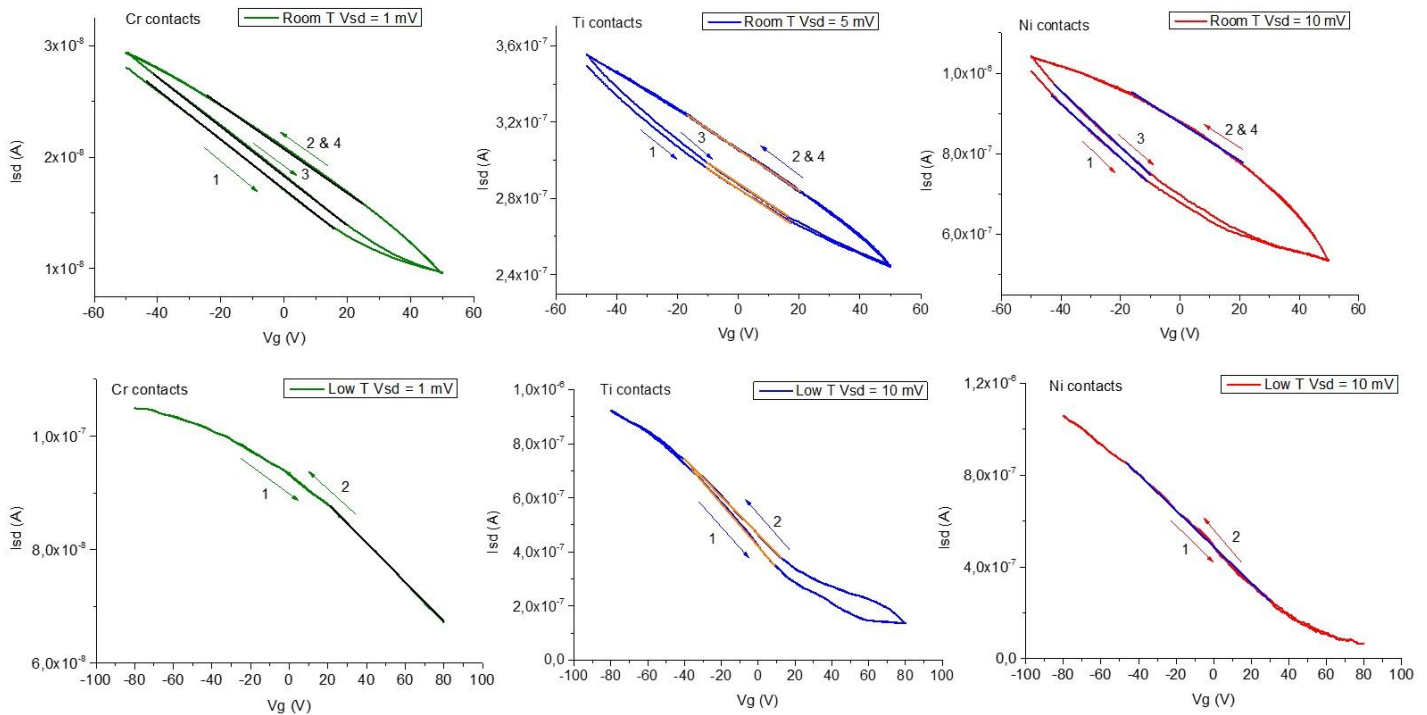


Figure 18: Source-drain current characteristics of our three samples at room and low temperature. Arrows give the direction of sweeping and numbers give the order of the sweeps. The coloured lines are a guide to the eye for the fitted linear regions for field-effect mobility evaluation.

At room temperature, these characteristics all display a hysteretic behaviour. We can also notice an inner loop in the second sweep, with all the contacting metals. This could be attributed to charge trapping at the contact interface or at the interface with the gate dielectric. Conversely, at low temperature this hysteretic behaviour vanishes except with titanium contacts. Since, in our case, the titanium deposition is far from being perfect, this result can be attributed to charge trapping in defects at the contact interface.

We can also see that the current modulation is quite low, generally about one order of magnitude. We do not see as well any ambipolar behaviour or saturation in the accumulation side for holes ( $V_g \ll 0$ ). This is why we cannot try to extract a value of the Schottky barrier of the contact with the method described in Chapter 1.

Several reasons could explain these results. First, our black phosphorus flakes are thicker than all those of the presented studies in Chapter 1. We do not know the exact value, but a comparison of the optical microscopy images clearly shows that our flakes are thicker. Moreover, we always used a 300 nm thick dielectric as gate oxide. By contacting thinner flakes and using a thinner dielectric, those curves could be more similar to those shown in figure 7 & 8.

We also use a back gate and our flakes are contacted on the top. Thus, the back gate voltage mainly modulates the bottom layers and we inject the carriers from the top layers. This is the

case of most of the described paper such as [7], where some considerations on thickness-dependence of the modulation are given.

In accumulation region, as shown in [19], if it is true that the back gate modulates preferentially the bottom layers, it is also true that they dominate the conduction, so the system has a 2D nature. In a linear-linear plot of  $I_{SD}$  vs  $V_g$  we do not see any clear saturation of the current in accumulation regime, and we also never see any saturation on the accumulation side for holes in figure 18.

On the other hand, a highly positive back gate voltage does not modulate the top layers and a hole current is flowing in these layers. Therefore, the electron current created in the gated bottom layer is hidden by the hole current in the top layers (where we inject and collect our carriers). This was observed by V. Tayari et al. in [20], where, in a thick black phosphorus flake with both top and bottom gate, they achieve a sort of vertical p-n junction. Electrons never become the majority carriers in the whole flake so that we never observe an ambipolar behaviour.

Concerning the unipolar behaviour observed, we could also have black phosphorus Fermi level pinning close to the valence band due to defects at contact interface, as it has been observed by L. Li et al. in a black phosphorus FET with Scandium contacts [21].

From these curves, the field-effect mobility is given by :

$$\mu_{FE} = \frac{dI_{SD}}{dV_g} \frac{L}{W} \frac{1}{C_{OX} V_{SD}} \quad (4)$$

where  $L$  and  $W$  are the length and the width of the channel in m, respectively. We do not take the length and width of the gate because the gate is covering the whole flake. Thus we use the effective dimensions where the current is flowing.  $C_{OX}$  is the oxide capacitance  $F/m^2$ ,  $I_{SD}$  is the source-drain current in A,  $V_{SD}$  and  $V_g$  the source-drain voltage and the gate voltage in V, respectively. To use this formula, we assume that the gate capacitance does not vary with the back gate voltage.

We can also calculate the mobility from the 4-probe conductance ( $G$ ) versus back gate voltage curves, obtained by measuring the 4-probe resistance versus  $V_g$ . A typical  $G$  vs  $V_g$  curve is shown in figure 19.

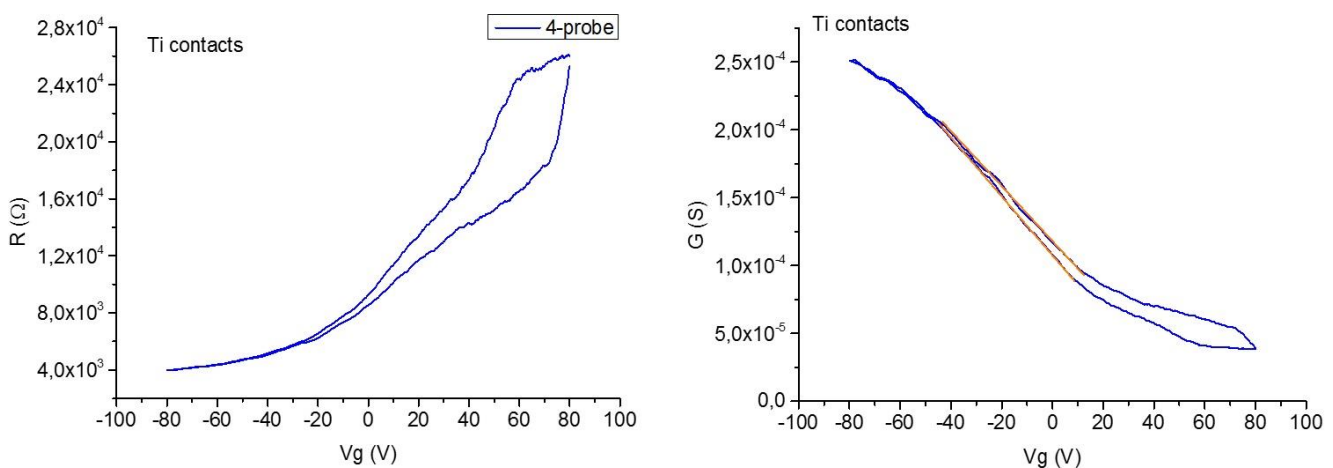


Figure 19:  $R$  vs  $V_g$  (left) and  $C$  vs  $V_g$  (right) characteristics of the Ti-contacted device from figure 17. Colored lines on  $G$  vs  $V_g$  graph are a guide to the eye of the fitted linear region for field-effect mobility.

From these curves, the field-effect mobility is given by :

$$\mu_{FE} = \frac{dG}{dV_g} \frac{L}{W} \frac{1}{C_{OX}} \quad (5)$$

where G is the conductance in S. Calculating the field-effect mobility from this measurement allows us to avoid complications due to contacts. We here get the mobility of carriers only in the channel.

Table 3 gathers calculated field-effect mobility values for different samples. When we have hysteretic curves, an average between the two fits is done.

Table 3: Field-effect mobility of three different samples. All the values are in  $\text{cm}^2/(\text{V.s})$ .

	$I_{SD}$ vs $V_g$	G vs $V_g$
Ti Room Temperature	61,51	160,11
Ti Low Temperature	216,43	563,37
Cr Room Temperature	23,46	39,21
Cr Low Temperature	101,46	-
Ni Room Temperature	78,30	223,51
Ni Low Temperature	391,17	1252,16

We can see that values obtained from the conductance measurement are higher, meaning that contacts have a real influence on the transport in the transistor (this is also what is observed with the other contacting metals). We also find higher mobilities at low temperature. This results from the reduced electron-phonon interactions and electrons-electrons interactions at low temperature. The field-effect mobility was also found to be strongly dependent on the thickness of the flake in the literature [7].

From these results, we can see that in the case of a thick black phosphorus flake, the contacting metal does not have a real influence on the behaviour of the transistor. The dominant conduction remains p-type no matter the contacting metal and this could be explained by Fermi level pinning near the valence band at the contact or because our top layers are not gated with a back gate. The temperature trend of the field-effect mobility is in good agreement with what is found in the literature. Among all the measured sample, calculated field-effect mobility lies in a wide range, from less than  $100 \text{ cm}^2/(\text{V.s})$  to  $\sim 400 \text{ cm}^2/(\text{V.s})$  at room temperature and from  $\sim 100 \text{ cm}^2/(\text{V.s})$  to  $\sim 1200 \text{ cm}^2/(\text{V.s})$  at low temperature (from G vs  $V_g$  curves). This scattering may be due to different oxidation states of the flakes (inducing more defects if oxidized), different thicknesses and also different crystallographic orientations of the flake (bP is a strongly anisotropic material).



## 4 Summary

### 4.1 Conclusion

Black phosphorus is an interesting material for many of its properties, in particular its layered structure allowing to exfoliate few layers and its high carriers mobility. This allows building high-performance low sized devices, such as field-effect transistors (FETs) for example. However, performances of such devices are strongly dependent on the behaviour of the interface with the contacting metal. This is what was investigated in this study, to try to find the best contacting metal among chromium, titanium and nickel.

We can first state that fabrication with this reactive material is quite difficult and this influences the measurements. It is also difficult to get really thin black phosphorus flakes and this seems to influence a lot the behaviour of a device.

From the results obtained here, nickel appears to be the best candidate to get reliable and low resistive contacts. Further measurements are still under analysis to try to have a better characterization of the behaviour of the contact depending on the metal.

From the literature, we can also see that the contacting metal has an influence on the behaviour of the transistor when we modulate the number of carriers, but this was not demonstrated by the measurements presented here.

Overall, chromium seems to give reliable and performant contacts, but our results with this metal were influenced by the resistivity of black phosphorus under the contact. With titanium we theoretically get a Schottky contact, and we here observe higher contact resistances with this metal. Moreover, it is more reactive than chromium and nickel, what makes it difficult to deposit in a reliable way. More scattering in the results were observed with titanium. Finally, nickel seems to give the lowest contact resistances, due to its ohmic contact it creates with black phosphorus, but it could affect the ambipolar behaviour of the transistor according to the literature. The nature of the contacts are to be confirmed with the further measurements still under analysis.

Results presented here are important for further studies with black phosphorus. The literature background about this material is quite low compared to other 2D semiconductors usually studied like graphene or TMDs. This work can bring some further answer to the community working with black phosphorus.

Many further studies can still be done with this material to try to get a complete framework of its behaviour. Some simulations to model the metal-black phosphorus contact and the carrier injections at the interface would also be helpful to complete this work.



## References

- 1 Y. Cai, G. Zhang, Y.-W. Zhang. *Layer-Dependent Band Alignment and Work Function of Few-Layer Phosphorene*. Scientific Reports. 2014.
- 2 W. S. Leong, X. Luo et al. *Low Resistance Metal Contacts to MoS<sub>2</sub> Devices with Nickel-Etched-Graphene Electrodes*. ACS Nano. 2015.
- 3 Morita, A. *Semiconducting Black Phosphorus*. Applied Physics A Solids and Surfaces. 1986.
- 4 X. Ling, H. Wang, et al. *The Renaissance of Black Phosphorus*. Proceeding of the National Academy of Sciences. 2015.
- 5 S. Das, W. Zhang, et al. *Tunable Transport Gap in Phosphorene*. Nano Letters. 2014.
- 6 B. Kiraly, N. Hauptmann et al. *Probing Single Vacancies in Black Phosphorus at the Atomic Level*. Nano Letters. 2017.
- 7 L. Li, Y. Yu, et al. *Black Phosphorus Field-Effect Transistor*. Nature Nanotechnology. 2014.
- 8 K. S. Novoselov, A. K. Geim. *Electric Field Effect in Atomically Thin Carbon Films*. Science. 2004.
- 9 A. Favron, E. Gaufrès, et al. *Photoxydation and Quantum Confinement Effects in Exfoliated Black Phosphorus*. Nature Materials. 2015.
- 10 D. J. Perello, S.H. Chae et al. *High-performance n-type black phosphorus transistors with type control via thickness and contact metal engineering*. Nature Communications. 2015.
- 11 Y. Du, H. Liu et al. *Device Perspective for Black Phosphorus Field-effect Transistors: Contact Resistance, Ambipolar Behavior and Scaling*. ACS Nano. 2014.
- 12 Y. Ma, C. Shen, et al. *Black-Phosphorus Field-Effect Transistors with Work Function Tunable Contacts*. ACS Nano. 2017.
- 13 A. Allain, J. Kang et al. *Electrical contacts to two-dimensional semiconductors*. Nature Materials. 2015.
- 14 S. Das, M. Demarteau et al. *Ambipolar Phosphorene Field-Effect Transistor*. ACS Nano. 2014.
- 15 H. Liu, A. T. Neal et al. *Phosphorene: An Unexplored 2D Semiconductor with a High Hole Mobility*. ACS Nano. 2014.
- 16 D. Xang, C. Han et al. *Surface transfer doping induced effective modulation on ambipolar characteristics of few-layer black phosphorus*. Nature Communications. 2015.
- 17 D. R. Lide. *CRC Handbook of Chemistry and Physics*. CRC Press/Taylor and Francis. 2008.
- 18 A. Favron, E. Gaufrès et al. *Photooxidation and Quantum Confinement Effects in Exfoliated Black Phosphorus*. Nature Materials. 2015.
- 19 V. Tayari, N. Hemsworth et al. *Two-Dimensional Magnetotransport in a Black Phosphorus Naked Quantum Well*. Nature Communications. 2015.
- 20 V. Tayari, N. Hemsworth et al. *Dual-Gate Velocity-Modulated Transistor Based on Black Phosphorus*. Physical Review Applied. 2016.
- 21 L. Li, M. Engel et al. *High-Performance p-Type Black Phosphorus Transistor with Scandium Contacts*. ACS Nano. 2016.

22 S. T. Koenig, R. A. Doganov et al. *Electric Field Effect in Ultrathin Black Phosphorus*.  
Applied Physics Letters. 2014.

## 4.2 Abstract

Building low sized and performant devices is crucial for the future of electronics. Black phosphorus is a good candidate to build field-effect transistors from many of its properties and understanding the behaviour at the interface with the metal is crucial to build reliable devices. In this study, we propose to test three different contacting metals to black phosphorus, Chromium, Titanium and Nickel, in order to find a good contacting metal for black phosphorus field-effect transistors. From the work presented here, Nickel seems to be the best candidate, giving reliable and ohmic contacts with the lowest contact resistance. Titanium seems to be the one to avoid from this point of view, giving more scattering and less reliability due to its high reactivity and its difficulty to be evaporated properly. It also gives the highest contact resistance, due to oxidation layers that may be present at the interface and a Schottky behaviour for carriers injection.

Finally, transport measurements display an unipolar p-type behaviour for bP FETs with the three metals on thick black phosphorus flakes at room and helium temperature. Field-effect mobility was also found to be higher at low temperature, in good agreement with what was already reported in literature.

## 4.3 Résumé

Depuis quelques décennies, les matériaux 2D ont attiré l'attention des chercheurs pour leur propriétés particulières et la possibilité de les inclure dans des appareils de très petite taille. Le phosphore noir est un matériaux semiconducteur permettant l'exfoliation d'un plan monoatomique. Il est donc intéressant pour construire des dispositifs électroniques tels que des transistor à effet de champ. Pour obtenir de tels dispositifs performants, il est important de comprendre le comportement de la jonction entre le métal et le phosphore noir.

Dans cette étude, trois différents métaux sont testés, chrome, titane et nickel dans le but de trouver celui qui permet la meilleure injection des porteurs dans le canal du transistor.

D'après les résultats présentés, le nickel semble être le métal donnant la plus faible résistance de contact grâce au comportement ohmique de la jonction. Le titane apparaît comme celui à éviter car il donne la plus grande résistance de contact, mais aussi à cause de la difficulté à le déposer correctement de part sa réactivité.

Les mesures de transport électronique sur des échantillons de phosphore noir épais montre un comportement unipolaire du transistor, où les trous sont les porteurs majoritaires à température ambiante et à basse température. La mobilité des porteurs de charges calculée à partir de ces mesures est plus grande à basse température qu'à température ambiante, conformément avec ce qui était déjà observé dans la littérature.